Article

Cell Metabolism

Cytosolic Aspartate Availability Determines Cell Survival When Glutamine Is Limiting

Graphical Abstract

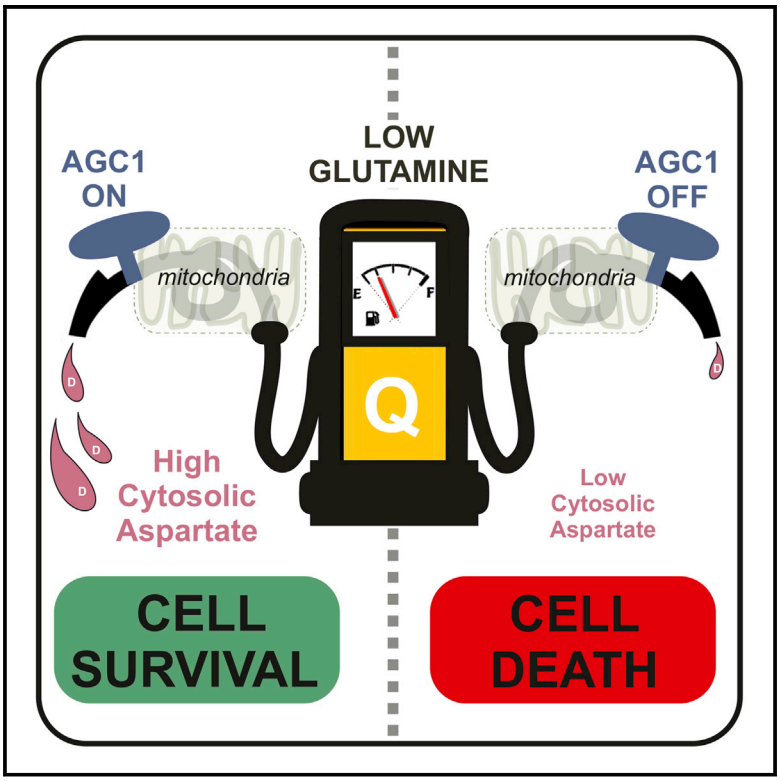

Highlights

- Cells lacking the mitochondrial aspartate exporter (AGC1) require glutamine metabolism
- Cytosolic aspartate is required to sustain survival when glutamine is limiting
- Glutamine anaplerosis supports aspartate production
- AGC1 loss sensitizes tumors to glutaminase inhibition *in vivo*

Authors

H. Furkan Alkan, Katharina E. Walter, Alba Luengo, ..., Tobias Madl, Matthew G. Vander Heiden, Juliane G. Bogner-Strauss

Correspondence

mvh@mit.edu (M.G.V.H.), juliane.bogner-strauss@tugraz.at (J.G.B.-S.)

In Brief

Alkan et al. show that, under conditions in which cytosolic glutamine is limiting, mitochondrial aspartate export, via the aspartate-glutamate carrier 1 (AGC1), supports cell proliferation and cellular redox homeostasis and that AGC1 inhibition can synergize with glutaminase inhibition to limit tumor growth.

Alkan et al., 2018, Cell Metabolism *28*, 706–720
November 6, 2018
https://doi.org/10.1016/j.cmet.2018.07.021

CellPress

CellPress

Cell Metabolism
Article

Cytosolic Aspartate Availability Determines Cell Survival When Glutamine Is Limiting

H. Furkan Alkan,[1,2] Katharina E. Walter,[1] Alba Luengo,[2] Corina T. Madreiter-Sokolowski,[3] Sarah Stryeck,[3] Allison N. Lau,[2] Wael Al-Zoughbi,[4] Caroline A. Lewis,[5] Craig J. Thomas,[6,7] Gerald Hoefler,[4,8] Wolfgang F. Graier,[3,8] Tobias Madl,[3,8] Matthew G. Vander Heiden,[2,9,*] and Juliane G. Bogner-Strauss[1,8,10,*]

[1]Institute of Biochemistry, Graz University of Technology, Humboldtstrasse 46/III, 8010 Graz, Austria
[2]The Koch Institute for Integrative Cancer Research and Department of Biology, Massachusetts Institute of Technology, Cambridge, MA 02139, USA
[3]Gottfried Schatz Research Center, Molecular Biology and Biochemistry, Medical University of Graz, Neue Stiftingtalstrasse 6/6, A-8010 Graz, Austria
[4]Diagnostic and Research Institute of Pathology, Medical University of Graz, Neue Stiftingtalstraße 6, A-8010 Graz, Austria
[5]Whitehead Institute for Biomedical Research, 455 Main Street, Cambridge, MA 02142, USA
[6]Division of Preclinical Innovation, National Center for Advancing Translational Sciences, National Institutes of Health, Bethesda, MD 20892, USA
[7]Lymphoid Malignancies Branch, National Cancer Institute, Bethesda, MD 20892, USA
[8]BioTechMed-Graz, Graz, Austria
[9]Dana-Farber Cancer Institute, Boston, MA 02115, USA
[10]Lead Contact
*Correspondence: mvh@mit.edu (M.G.V.H.), juliane.bogner-strauss@tugraz.at (J.G.B.-S.)
https://doi.org/10.1016/j.cmet.2018.07.021

SUMMARY

Mitochondrial function is important for aspartate biosynthesis in proliferating cells. Here, we show that mitochondrial aspartate export via the aspartate-glutamate carrier 1 (AGC1) supports cell proliferation and cellular redox homeostasis. Insufficient cytosolic aspartate delivery leads to cell death when TCA cycle carbon is reduced following glutamine withdrawal and/or glutaminase inhibition. Moreover, loss of AGC1 reduces allograft tumor growth that is further compromised by treatment with the glutaminase inhibitor CB-839. Together, these findings argue that mitochondrial aspartate export sustains cell survival in low-glutamine environments and AGC1 inhibition can synergize with glutaminase inhibition to limit tumor growth.

INTRODUCTION

Proliferation increases the energetic and biosynthetic needs of cells. To meet these demands, proliferating cells alter their metabolism and utilize nutrients differently than non-proliferating cells (Vander Heiden and DeBerardinis, 2017; Cantor and Sabatini, 2012; Warburg, 1956). In culture, most proliferating cells depend on two main carbon sources: glucose and glutamine (Hosios et al., 2016). Although oxidative glucose catabolism is energetically the most efficient means to produce ATP, proliferating cells often exhibit increased lactate production—also known as aerobic glycolysis (Cantor and Sabatini, 2012; Vander Heiden et al., 2009). In addition, glutamine is a primary anaplerotic tricarboxylic acid (TCA) cycle substrate for many cells, making those cells vulnerable to glutamine withdrawal or glutaminase inhibition by drugs such as CB-839 (Gross et al., 2014; Yuneva et al., 2007).

Despite prominent lactate production, mitochondrial function remains important for proliferating cells (DeBerardinis and Chandel, 2016). Mitochondrial one-carbon metabolism is strongly upregulated in many cancer types to maintain purine and thymidine biosynthesis (Vyas et al., 2016; Zong et al., 2016). Initiating *de novo* lipogenesis in mitochondria through citrate production is also vital for proliferation in some contexts (Catalina-Rodriguez et al., 2012; Jiang et al., 2017). Another important role for mitochondrial respiration in proliferating cells is to support aspartate production, as aspartate is essential to make protein as well as for purine and pyrimidine biosynthesis (Birsoy et al., 2015; Gui et al., 2016; Sullivan et al., 2015). Because of these biosynthetic roles of mitochondria, movement of macromolecule precursors across the mitochondrial membranes might also become a limitation for tumor growth. For instance, blocking the mitochondrial citrate transporter impairs *de novo* lipogenesis and inhibits cell proliferation in some contexts (Catalina-Rodriguez et al., 2012). In addition, transferring electrons between the cytosolic and mitochondrial compartments may also be important because accumulation of reducing equivalents in either compartment could cause proliferation defects. For instance, inhibiting mitochondrial electron transport leads to NADH accumulation in mitochondria, which hampers oxidation reactions, impairs aspartate synthesis, and slows proliferation (Sullivan et al., 2015). Regenerating cytosolic NAD+ is also vital for glycolysis and the biosynthesis of certain amino acids and nucleotides (Lunt and Vander Heiden, 2011). Therefore, understanding the role of mitochondrial transporters in proliferating cells could not only provide insight into cancer metabolism, but also suggest novel cancer drug targets.

The malate-aspartate shuttle (MAS) is important for transferring electrons from cytosolic NADH to the mitochondria, where they can be transferred to oxygen via the electron transport

chain (Greenhouse and Lehninger, 1976). Exchange of mitochondrial aspartate for cytosolic glutamate and a proton by the aspartate-glutamate carrier (AGC) is proposed to be the only irreversible step of the MAS (del Arco et al., 2002). Both AGC isoforms are predicted to be functionally identical (Thangaratnarajah et al., 2014), yet many tissues selectively express one isoform: AGC1 (*SLC25A12*, Aralar) is abundant in brain, skeletal muscle, and pancreatic beta cells, while AGC2 (*SLC25A13*, Citrin) is primarily found in liver and kidney (Begum et al., 2002; Palmieri et al., 2001). Previous studies have shown that AGC1 is involved in neuronal development, supports aspartate and N-acetylaspartate production, and reduces lactate secretion (Jalil et al., 2005; Rubi et al., 2004).

Although MAS activity in tumors has been reported (Greenhouse and Lehninger, 1976) and the expression of AGCs in cancer has been predicted (Amoedo et al., 2016), the functional importance of mitochondrial aspartate-glutamate transport in proliferating cells has not been extensively studied. Here, we show that AGC1 knockdown (KD) slows cell proliferation, reduces the cellular NAD+/NADH ratio, and impairs aspartate delivery to the cytosol. We also show that mitochondrial aspartate export is essential for cell survival in glutamine-limited conditions, and that loss of AGC1 can synergize with glutaminase inhibitors to suppress tumor growth. These findings argue that sustaining cytosolic aspartate levels is required for cell survival in low-glutamine environments and suggest that AGC1 might be a target to treat some cancers.

RESULTS

Knockdown of AGC1 Reduces Proliferation Due to Impaired Aspartate Synthesis

AGC1 exports aspartate produced in mitochondria to the cytosol, where it can be used for nucleotide, amino acid, and protein synthesis. In addition, mitochondrial aspartate export can contribute to cytosolic redox homeostasis by serving as a substrate for cytosolic glutamate-oxaloacetate transaminase (Got1, producing oxaloacetate from aspartate) and malate dehydrogenase (Mdh1, reducing oxaloacetate to malate while oxidizing NADH) as part of the MAS (Figures 1A and S1A). mRNA expression analysis suggests that proliferating cells in culture display robust expression of MAS components (Figure S1B).

To test whether AGC1 is important for cell proliferation, we used short hairpin RNA (shRNA) to knock down AGC1 in non-transformed mouse C2C12 myoblasts because AGC1 levels in these cells are about 8-fold higher than AGC2 levels (Figure S1B). We observed that AGC1-KD leads to a slight, yet significant, proliferation rate reduction when cells are cultured in standard DMEM containing 1 mM pyruvate (Figure 1B). Because extracellular pyruvate can act as an electron acceptor to provide oxidized NAD+ to cells (Figure 1A), we excluded pyruvate from the media for subsequent experiments unless otherwise indicated. The effect of AGC1-KD on cell proliferation becomes more apparent following pyruvate withdrawal, and this change is rescued by pyruvate or aspartate supplementation (Figure 1C), as reported previously for cells with mitochondrial dysfunction (Birsoy et al., 2015; Sullivan et al., 2015). Interestingly, however, AGC1-KD cells remain viable and retain the ability to proliferate slowly in pyruvate-free media (Figure 1C).

Disruption of the MAS is expected to decrease the NAD+/NADH ratio in the cytosol and increase the NAD+/NADH ratio in the mitochondria (del Arco et al., 2002). Indeed, the whole-cell NAD+/NADH ratio is lower in AGC1-KD cells compared to non-targeting control (NTC) cells, hereafter referred to as control cells (Figure 1D). In addition, because the lactate dehydrogenase reaction is coupled to cytosolic NAD+/NADH, the pyruvate/lactate ratio is sometimes used as a proxy for this ratio (Christensen et al., 2014; Williamson et al., 1967), and indeed AGC1-KD cells have a lower pyruvate/lactate ratio (Figure 1E). Basal oxygen consumption rate is also lower in AGC1-KD cells (Figure 1F), a finding that is consistent with the expected increase in mitochondrial NAD+/NADH ratio. To determine whether AGC1-KD leads to similar phenotypes in transformed cells, we examined mouse Lewis lung carcinoma (LLC1) cells. As observed in C2C12 cells, AGC1-KD LLC1 cells proliferate slower than control LLC1 cells and have reduced NAD+/NADH and pyruvate/lactate ratios (Figures S1C–S1E).

The low NAD+/NADH ratio of AGC1-KD cells is accompanied by reduced aspartate levels in both C2C12 and LLC1 cells (Figures 1G and S1F). To assess whether cytosolic aspartate is changed, we examined how AGC1-KD affects asparagine levels, an amino acid that is not present in the culture media, because the conversion of aspartate to asparagine is mediated by the cytosolic enzyme asparagine synthetase (Asns) (Ahn and Metallo, 2015). KD of AGC1 leads to reduced asparagine levels, indicative of lower cytosolic aspartate levels in these cells (Figures 1G and S1F).

We also tested the effects of increased AGC1 expression and found that overexpression of mouse AGC1 promotes C2C12 cell proliferation (Figure S1G). Increased expression of mouse AGC1 elevates whole-cell NAD+/NADH ratio and aspartate levels, the opposite of what was observed following AGC1 KD using three independent shRNAs (Figures S1H–S1J). Furthermore, expression of human AGC1 that is resistant to KD rescues the proliferation defect observed in AGC1-KD C2C12 cells (Figure S1K).

AGC1-KD Increases Cellular Dependence on Glutamine

We hypothesized that AGC1-deficient cells maintain proliferation by rewiring metabolism to obtain cytosolic aspartate from a different source. To test this hypothesis, we individually removed glucose or select amino acids from the media and assessed whether these interventions further affected cell proliferation upon AGC1 KD. We found that culturing cells in low glucose (0.5 mM, instead of 25 mM contained in regular DMEM) or with the glycolysis inhibitor 2-deoxyglucose (2-DG) does not affect proliferation or survival of AGC1-KD cells more than control cells (Figure 2A). However, survival of AGC1-KD cells was compromised more than control cells in Hank's Buffered Salt Solution (HBSS) that contains 5.5 mM glucose but lacks amino acids (Figure 2B). Addition of essential amino acids did not rescue this phenotype, but addition of essential amino acids and glutamine to HBSS was able to rescue AGC1-KD cell proliferation to the same degree as control cells (Figure 2B). To further explore whether AGC1-KD alters dependence on glutamine, we cultured cells in DMEM-based low-glutamine media (0.1 mM instead of 4 mM). In line with previous studies (Wise and Thompson, 2010), low glutamine impairs cell proliferation, but in contrast to control cells, AGC1-KD cell survival is compromised in

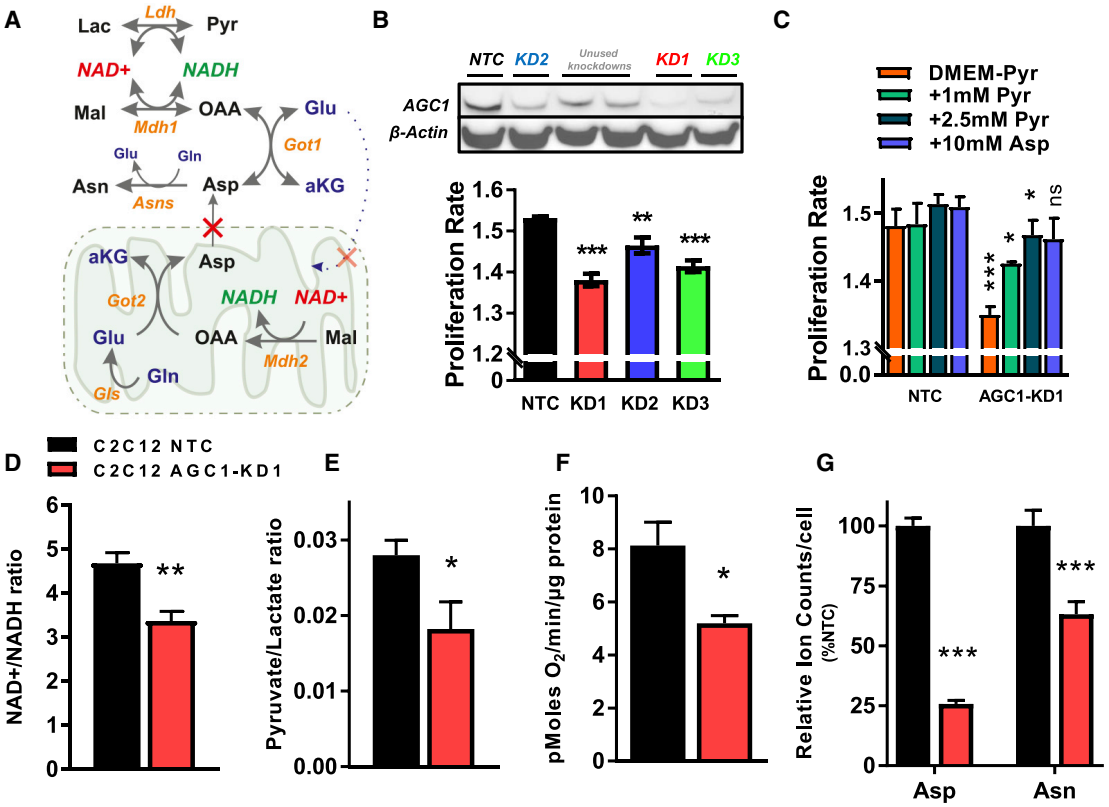

Figure 1. AGC1 Knockdown Decreases Cytosolic Aspartate Levels and Increases Dependence on Exogenous Electron Acceptors

(A) Schematic showing how aspartate can regenerate NAD+ in the cytosol through the MAS involving glutamate-oxaloacetate transaminase (Got1) and malate dehydrogenase (Mdh1).

(B) AGC1 KD in C2C12 cells using different shRNA hairpins was assessed by western blot as shown. Also shown is the fold change in viable cell number (proliferation rate) of control (NTC) and cells expressing three of the five hairpins (KD1, KD2, and KD3) as doublings/day (n = 3).

(C) Relative proliferation rate of control (NTC) and AGC1-KD1 C2C12 cells in the presence and absence of the indicated concentrations of pyruvate (Pyr) and aspartate (Asp) (n = 3).

(D) NAD+/NADH ratio of control (NTC) and AGC1-KD1 C2C12 cells cultured in pyruvate-free DMEM (n = 5). Means ± SEM are shown.

(E) Pyruvate to lactate ratio of control (NTC) and AGC1-KD1 C2C12 cells cultured in pyruvate-free media (n = 3).

(F) Mitochondrial oxygen consumption rate of control (NTC) and AGC1-KD1 C2C12 cells cultured in serum-free, phenol-red free media containing 5 mM glucose, 1 mM sodium pyruvate, and 2 mM glutamine (n = 3, each including 7–8 technical replicates).

(G) Relative cellular aspartate and asparagine levels of control (NTC) and AGC1-KD1 C2C12 cells cultured in standard DMEM without pyruvate (n = 3).

All figures denote mean ± SD unless indicated otherwise. *p ≤ 0.05, **p ≤ 0.01, ***p ≤ 0.001. See also Figure S1.

low-glutamine conditions (Figure 2C). Glutamine depletion (0.1 mM) significantly increased the percent of dead and apoptotic cells as measured by Annexin V/promidium iodide (PI) staining in both control and AGC1-KD cells (Figure S1L). Interestingly, AGC1-KD also induced cell death in glutamine-replete media that is further exacerbated by glutamine starvation (Figure S1L). Furthermore, cleaved caspase 3 levels, a marker of apoptotic cells, were increased in low-glutamine conditions, suggesting that glutamine starvation promotes cell death in AGC1-KD cells (Figure S1M).

Glutamine has several fates in cells: it can serve as an exchange factor for import of other amino acids (Pochini et al., 2014), it provides nitrogen for nucleotide biosynthesis (Cory and Cory, 2006), or it can be converted to α-ketoglutarate (α-KG, also known as 2-oxoglutarate) via glutamate to provide carbon for TCA cycle intermediates (anaplerosis) (Wise and Thompson, 2010) (Figure 2D). To narrow down which fate of glutamine is important for proliferation and viability of AGC1-KD cells, we used the glutaminase inhibitor CB-839 to limit glutamine to glutamate conversion. CB-839 treatment phenocopies the effects of culture in low glutamine on AGC1-KD cells (Figure 2C). These data argue that AGC1-KD cells require glutamine anaplerosis for survival, rather than for other downstream reactions that do not require glutaminase activity.

We next hypothesized that the increased vulnerability of AGC1-KD cells to glutaminase inhibition could be due to an inability to oxidize glucose. To test this, we treated C2C12 cells for 6 hr with CB-839 and measured oxygen consumption. Interestingly, CB-839 treatment reduces mitochondrial oxygen consumption by 50% in both AGC1-KD and control cells, arguing that AGC1-KD cells do not require more glutamine for mitochondrial respiration than control cells (Figure 3A). In addition, there is also no difference in the uptake or consumption rate of glucose and glutamine except that AGC1-KD C2C12 cells show slightly

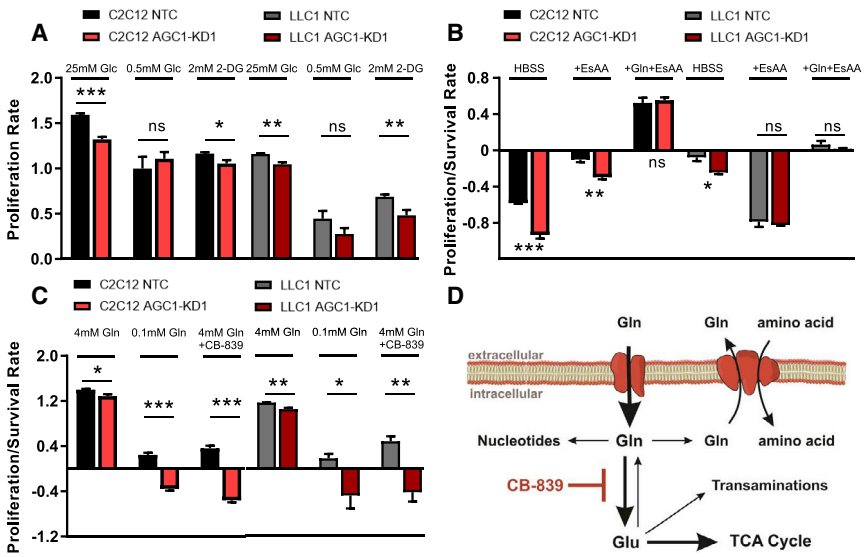

Figure 2. AGC1-KD Cells Are Sensitive to Glutamine Depletion

(A) Proliferation rate of control (NTC) and AGC1-KD (AGC1-KD1) C2C12 and LLC1 cells cultured in pyruvate-free DMEM containing 25 or 0.5 mM glucose (Glc), or 25 mM glucose and 2 mM 2-deoxyglucose (2-DG), as indicated (n = 5).

(B) Proliferation/survival rate of control (NTC) and AGC1-KD1 C2C12 and LLC1 cells cultured in pyruvate-free HBSS containing 5 mM glucose supplemented with 10% FBS and vitamins, with or without essential amino acids (EsAAs) and glutamine (Gln), as indicated (n = 3).

(C) Proliferation/survival rate of control (NTC) and AGC1-KD1 C2C12 and LLC1 cells cultured in pyruvate-free DMEM containing 4 or 0.1 mM glutamine (Gln), or 4 mM glutamine and 1 μM CB-839 (glutaminase inhibitor), as indicated (n = 5).

(D) Schematic showing some potential fates of glutamine in a cell.

All panels show mean ± SEM. *p ≤ 0.05, **p ≤ 0.01, ***p ≤ 0.001. See also Figure S1.

elevated glutamate release (Figures 3B, 3C, and S2A–S2C). Of note, only a small fraction of the consumed glutamine could be accounted for by glutamate excretion in either group, suggesting that the elevated glutamate excretion could be a consequence of an increased cytosolic glutamate pool in AGC1-KD cells and is not the cause of glutamine dependency. Consistent with this interpretation, exposure to Erastin, which inhibits activity of the plasma membrane glutamate exporter xCT (*Slc7a11*) (Dixon et al., 2014), has no specific impact on glutaminase-inhibited AGC1-KD cells (Figures S2D and S2E).

Hypoxia and mitochondrial dysfunction both alter the cell NAD+/NADH ratio and promote reductive glutamine metabolism (Metallo et al., 2011; Mullen et al., 2011, 2014; Sullivan et al., 2015). To determine whether AGC1-KD cells metabolize nutrients differently, we traced [U^{13}C]glucose or [U^{13}C]glutamine fates using gas chromatography-mass spectrometry (GC-MS). We did not observe a major change in labeling from either nutrient such that glutamine remains the predominant source of aspartate and other TCA intermediates, and the relative contribution of glucose and glutamine to the TCA cycle is not drastically altered in AGC1-KD cells (Figures S2F and S2G). However, in alignment with a high mitochondrial NAD+/NADH ratio, AGC1-KD C2C12 cells display decreased M+3 aspartate and M+5 citrate from labeled glutamine, consistent with decreased reductive α-KG carboxylation (Figures 3D and 3E). Moreover, at steady state, M+3 species of glutamate and α-KG are increased while M+5 species are decreased in AGC1-KD C2C12 cells without any major differences observed in unlabeled (M+0) species (Figures 3F and 3G). These labeling patterns are consistent with a higher mitochondrial NAD+/NADH ratio promoting increased oxidative TCA cycling (Figure 3H). Also consistent with this interpretation, AGC1-KD C2C12 cells release more ^{14}C-CO_2 from [U^{14}C]glutamine (Figures 3H and 3I). Interestingly, we did not observe the same decrease in reductive carboxylation in LLC1 cells with AGC1 KD (Figure S2G), suggesting that changes in reductive carboxylation are not why AGC-KD cells require glutamine. Together, these findings argue that, although changes are observed in the metabolism of AGC1-KD cells (Figures S2H–S2M), glutamine utilization is not drastically altered in AGC1-KD cells, and glutamine remains the major precursor for aspartate independent of AGC1 expression (Figures S2F and S2G).

AGC1-KD Cells Are Unable to Sustain Cytosolic Aspartate Levels, Leading to Cell Death upon Glutamine Deprivation

Because cytosolic aspartate production is essential for survival of cells with mitochondrial dysfunction (Birsoy et al., 2015), we hypothesized that aspartate export from mitochondria might be important to survive glutamine limitation. In fact, AGC1 protein expression is higher following glutamine deprivation, suggesting a higher demand for mitochondrial aspartate export in such conditions (Figure 4A). We reasoned that glutamine withdrawal might deplete mitochondrial aspartate levels such that other mitochondrial transporters cannot export it efficiently (Figure 4B). To test whether cytosolic aspartate delivery can be limiting for AGC1-KD cells in low glutamine, we provided cells with exogenous aspartate and found that aspartate supplementation in low-glutamine media rescues AGC1-KD cell viability and proliferation (Figures S3A and 4C). Because aspartate is poorly permeable, non-physiological aspartate concentrations (5–20 mM) are needed to deliver aspartate into the cells (Sullivan et. al., 2018). However, after expressing the aspartate transporter (SLC1A3), 150 μM aspartate was sufficient to rescue proliferation/survival in low-glutamine conditions (Figure S3B), arguing that cytosolic aspartate delivery can be limiting for AGC1-KD cells.

A requirement for glutamine in cells with AGC1 loss was observed in other cell lines, as was the ability of aspartate to rescue AGC1 loss, despite the fact that the cell lines showed varying responses to glutamine deprivation and glutaminase inhibition (Figure 4C). In addition, CRISPR/Cas9-mediated knockout of AGC1 leads to comparable sensitivity to perturbations that limit glutamine metabolism in C2C12 cells (Figure S3C). Interestingly, total ablation of AGC1 also did not completely block proliferation in glutamine-replete media, suggesting that

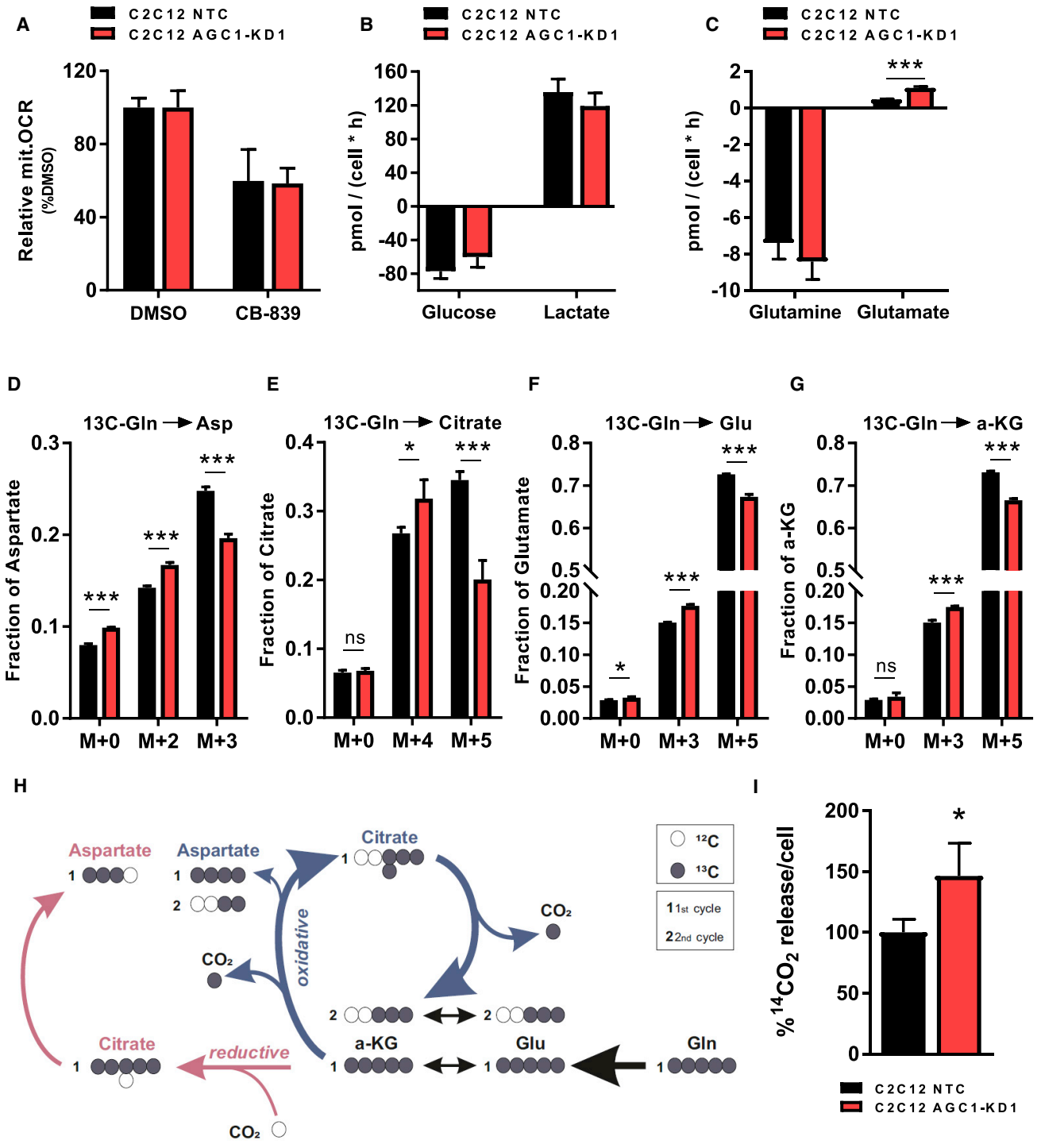

Figure 3. AGC1-KD Cells Exhibit Increased Oxidative TCA Cycle Metabolism

(A) Relative mitochondrial oxygen consumption rate (mit.OCR) of control (NTC) and AGC1-KD1 C2C12 cells cultured for 6 hr in pyruvate-free DMEM containing 4 mM glutamine with or without CB-839 (n = 5); data normalized to percent change compared to DMSO treatments of each group. Means ± SEM are shown.

(B and C) Uptake/consumption rate of glucose and lactate (B), and glutamine and glutamate (C) are shown for control (NTC) and AGC1KD C2C12 cells cultured in pyruvate-free DMEM for 48 hr (n = 3).

(D–G) Fractional labeling of aspartate (Asp) (D), citrate (E), glutamate (Glu) (F), and α-ketoglutarate (α-KG) (G) following culture of C2C12 control (black) or C2C12 AGC1-KD1 (red) cells (as in A–C) in media containing [U^{13}C]glutamine (Gln) for 24 hr (n = 3).

(legend continued on next page)

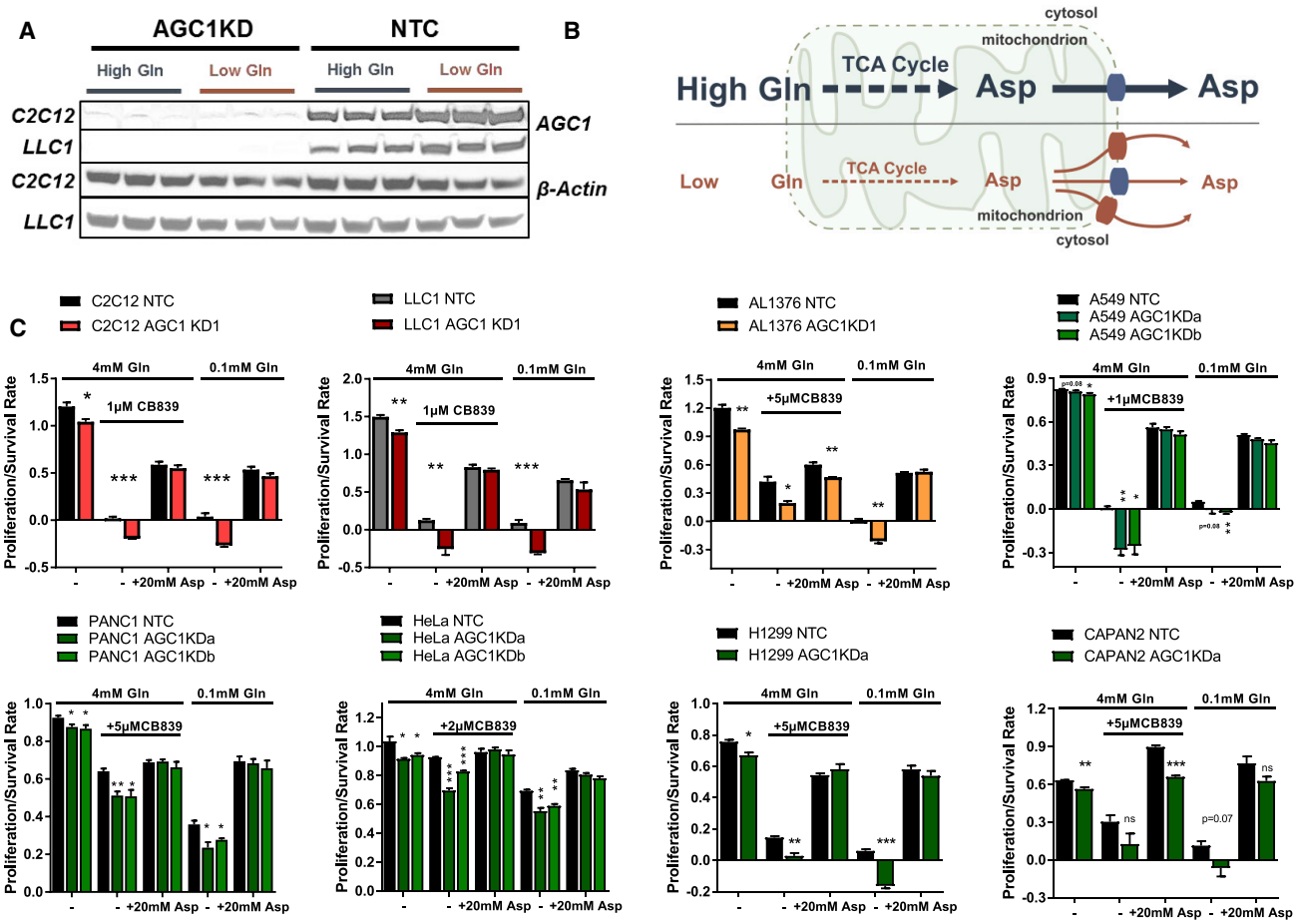

Figure 4. Cytosolic Aspartate Delivery Improves Proliferation/Survival Following Glutamine Limitation

(A) Western blot analysis of AGC1 protein expression in whole-cell lysates (40 μg/lane) from AGC1 KD (AGC1KD) or control (NTC) C2C12 or LLC1 cultured in DMEM with 10% FBS and 4 mM glutamine (High Gln) or 0.1 mM glutamine (Low Gln) for 24 hr as indicated.

(B) Schematic depicting how low glutamine might lead to reduced cytosolic aspartate delivery and increased aspartate transporter expression.

(C) Proliferation/survival rate of control (NTC) and AGC1KD C2C12, LLC1, AL1376, A549, PANC1, HeLa, H1299, and CAPAN2 cells cultured in pyruvate-free DMEM containing 4 or 0.1 mM glutamine (Gln), or 4 mM glutamine with CB839 at the specified concentrations in the presence or absence of 20 mM aspartate (Asp), as indicated (n = 3). Mean ± SEM.

*p ≤ 0.05, **p ≤ 0.01, ***p ≤ 0.001. See also Figure S3.

some cytosolic aspartate delivery is sustained by AGC2 or other mitochondrial transporters when glutamine is present. Of note, glutamate supplementation failed to completely rescue AGC1-KD cells in low-glutamine conditions, suggesting that reduced mitochondrial glutamate uptake may be one factor exacerbating the dependence of AGC1-KD cells on glutamine anaplerosis (Figures S3D and S3E).

AGC1-KD Cells Require High Mitochondrial Aspartate Levels to Maintain Aspartate Export

We next hypothesized that AGC1-deficient cells require high mitochondrial aspartate levels to maintain sufficient aspartate delivery to the cytosol. Therefore, we examined whether AGC1-KD cells are vulnerable to other perturbations that deplete mitochondrial aspartate. Metformin blocks mitochondrial aspartate production by inhibiting mitochondrial complex I and consequently disrupting the NAD+/NADH ratio (Sullivan et al., 2015) (Figure 5A), and AGC1-KD cells are more sensitive to metformin treatment than control cells (Figure 5B). Furthermore, other anaplerotic carbon sources might support mitochondrial aspartate production (Figure 5A), and both daKG and pyruvate supplementation improve proliferation/survival of AGC1-KD cells in glutamine limitation (Figure 5C) and increase aspartate levels (Figures 5D and S4A–S4D). These findings suggest that limiting

(H) Schematic overview of oxidative and reductive glutamine catabolism highlighting how labeled carbons from glutamine (Gln) label glutamate (Glu), α-ketoglutarate (α-KG), and the other indicated metabolites.

(I) Relative $^{14}CO_2$ release from control (NTC) and AGC1-KD C2C12 cells cultured in media containing [U^{14}C]-glutamine for 1 hr (n = 3).

All figures show mean ± SD unless indicated otherwise. *p ≤ 0.05, **p ≤ 0.01, ***p ≤ 0.001. See also Figure S2.

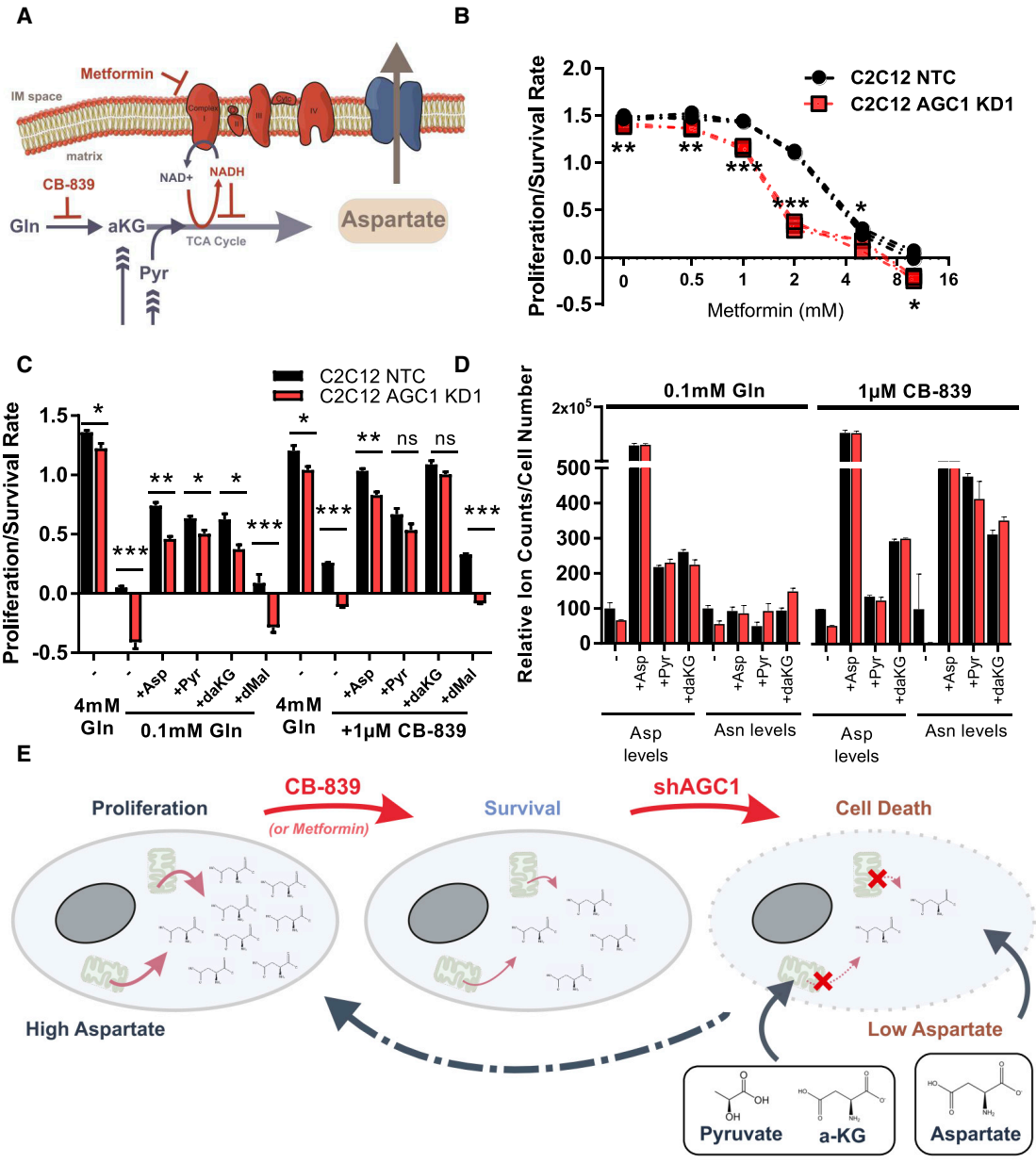

Figure 5. Sustaining Cytosolic Aspartate Levels Prevents Cell Death in Glutamine-Limiting Conditions

(A) Schematic showing how glutamine and alternative anaplerotic substrates can fuel the TCA cycle and support mitochondrial aspartate synthesis. How CB-839-mediated inhibition of glutaminase and metformin inhibition of NAD+ regeneration affect TCA cycling are also shown.

(B) Proliferation/survival rate of control (NTC) and AGC1-KD C2C12 cells treated with varying concentration of metformin in pyruvate-free DMEM (n = 3).

(C) Proliferation/survival rate of control (NTC) and AGC1-KD C2C12 cells cultured in 4 or 0.1 mM glutamine, or 4 mM glutamine with 1 μM CB-839, in the presence or absence of 20 mM aspartate (Asp), 2 mM sodium pyruvate (Pyr), 2 mM dimethyl-α-ketoglutarate (daKG), or 2 mM dimethylmalate (dMal), as indicated (n = 3).

(D) Relative cellular aspartate and asparagine levels in control (NTC) and AGC1-KD C2C12 cells cultured in 0.1 or 4 mM glutamine with 1 μM CB-839 in the presence or absence of 20 mM aspartate (Asp), 2 mM sodium pyruvate (Pyr), or 2 mM dimethyl-α-ketoglutarate (daKG), as indicated (n = 3).

(E) Schematic depicting a model for how changes in cytosolic aspartate levels might correlate with cell survival.

All figures denote means ± SEM unless indicated otherwise. *p ≤ 0.05, **p ≤ 0.01, ***p ≤ 0.001. See also Figure S4.

glutamine anaplerosis for aspartate production decreases mitochondrial and cytosolic aspartate levels and inhibits cell proliferation. In AGC1-KD cells, however, the inability to export residual aspartate from mitochondria further reduces cytosolic aspartate and compromises cell proliferation and cell survival (Figure 5E).

Cytosolic Aspartate Is Essential for Nucleotide Biosynthesis, but Not for Non-essential Amino Acids or the TCA Cycle

Aspartate is a proteinogenic amino acid that is also involved in several metabolic pathways beyond its use for protein synthesis,

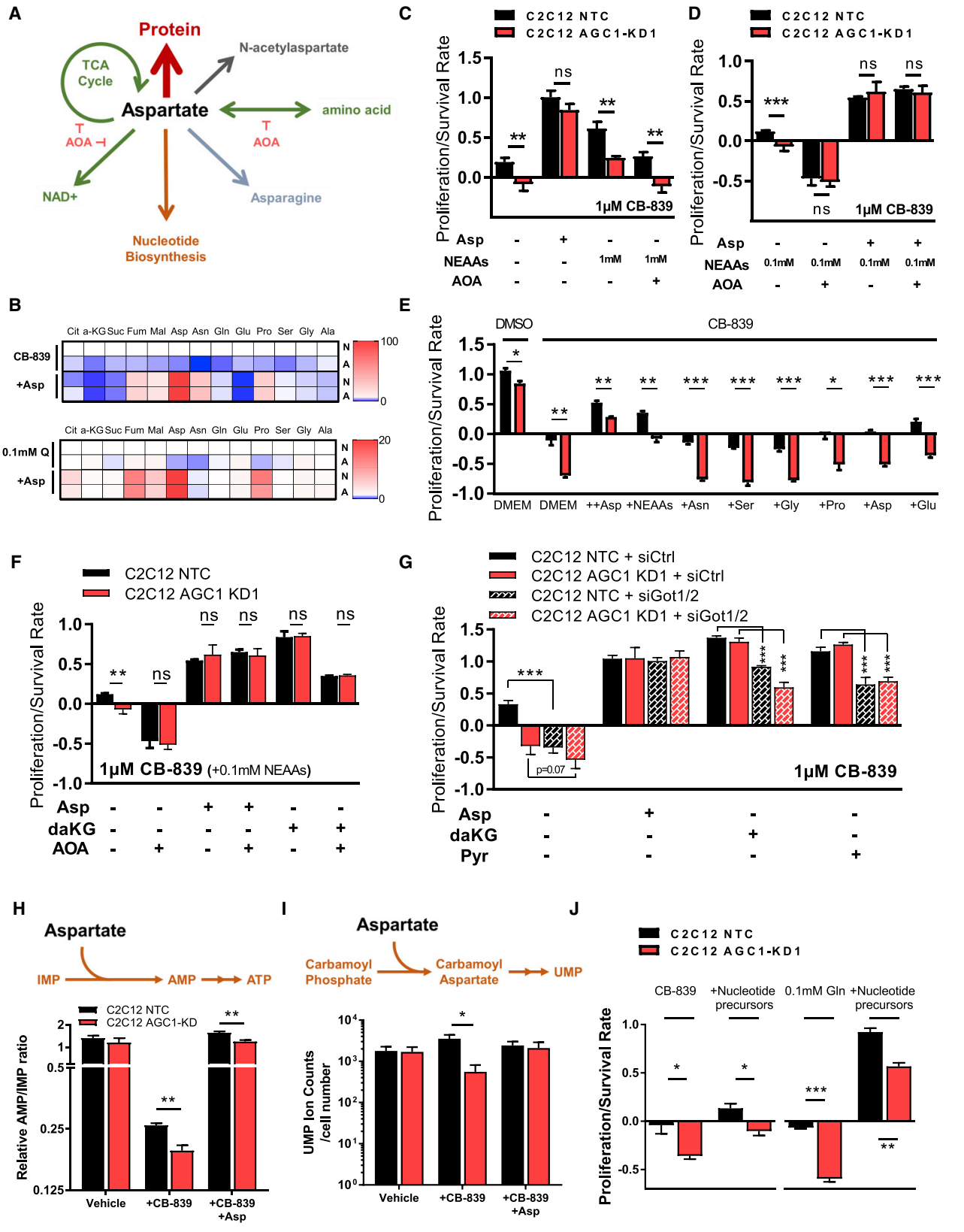

(legend on next page)

some of which have been reported to be associated with cell proliferation (Birsoy et al., 2015; Krall et al., 2016; Sullivan et al., 2015; Zand et al., 2016) (Figure 6A). Cytosolic aspartate could undergo transamination to support non-essential amino acid (NEAA) synthesis, deliver four carbon units to mitochondria for use in the TCA cycle, or recycle NAD+ through the cytosolic part of the MAS. In addition to fates involving transamination, aspartate can accept an amide nitrogen from glutamine for asparagine biosynthesis, is essential for both purine and pyrimidine biosynthesis, and is acetylated to produce N-acetylaspartate (NAA), a brain metabolite that may have roles outside of the central nervous system (Figure 6A). Although NAA was recently reported to have beneficial effects on survival of some cancer cells (Bogner-Strauss, 2017; Lou et al., 2016; Zand et al., 2016), we failed to detect endogenous NAA in either C2C12 or LLC1 cells, suggesting that production of NAA cannot explain why cytosolic aspartate is a limitation for the cells studied here (Figures S5A and S5B).

To explore the role of cytosolic aspartate in NEAA synthesis, we first checked mRNA expression of enzymes involved in amino acid metabolism in low-glutamine conditions. Glutamine starvation (0.1 mM) alters expression of many transaminases regulated by activating transcription factor 4 (*Atf4*), a component of the amino acid starvation response (Chen et al., 2014) (Figure S5C). Interestingly, the expression of genes encoding enzymes that would use aspartate in the cytosol (*Got1* and *Asns*), but not in the mitochondria (*Got2*), is upregulated in low-glutamine conditions (Figure S5C). Other cytosolic transaminase isoforms are also upregulated, while mitochondrial isoforms of the same transaminases remain unchanged or are downregulated (Figure S5C). This suggests that cytosolic transamination could be more important following glutamine limitation. In fact, levels of NEAAs (except for serine and glycine that are present in DMEM) are reduced upon CB-839 treatment or in low glutamine (Figure S4A) and are lower in AGC1-KD cells compared to control cells, which is partially rescued by aspartate supplementation (Figure 6B). However, because transamination reactions are highly reversible and the transfer of nitrogen between amino acids is not uni-directional (Wiechert, 2007), NEAAs might also be consumed to make aspartate when aspartate levels drop upon glutamine withdrawal.

To test whether aspartate or other NEAAs are necessary to rescue cells in glutamine limitation, we provided cells with either a mixture of NEAAs or aspartate, in the presence or absence of the transaminase inhibitor aminooxyacetate (AOA) (Figure S5D). Similar to aspartate, high levels of NEAAs rescue AGC1-KD cells following glutaminase inhibition; however, this rescue is blunted by AOA, suggesting that NEAA rescue of glutaminase inhibition requires transamination (Figures 6C, 6D, S5E, and S5F). Of note, a 0.1 mM mixture of NEAAs was included when cells were treated with AOA as transaminase activity is needed to produce other NEAAs, and complete loss of NEAAs might impact proliferation/survival even when glutamine is not limiting (Figures 6D, S5E, and S5F). Notably, none of the amino acids, including asparagine, can rescue glutaminase inhibition individually, except for a partial rescue by glutamate, which is itself the product of glutaminase (Figures 6E and S5G). On the other hand, AOA treatment reduces the survival of control cells to the level of AGC1-KD cells upon CB-839 treatment (Figures 6D, S5E, and S5F). Importantly, AOA treatment did not affect proliferation/survival of cells rescued with aspartate, arguing that aspartate does not require transamination to rescue glutamine limitation. These data suggest that aspartate is an essential end product of transamination reactions and is not particularly limiting for NEAA synthesis when glutamine anaplerosis is inhibited.

Figure 6. Cytosolic Aspartate Is Limiting for Nucleotide Biosynthesis When Glutamine Metabolism Is Compromised

(A) Schematic showing the potential fates of cytosolic aspartate. Aspartate is a proteinogenic amino acid (red) that could undergo transaminations (green) to support NEAA biosynthesis, oxidize cytosolic NADH through MAS, and provide carbon for the mitochondrial TCA cycle. Aspartate can also be a precursor to produce asparagine (blue), be acetylated to produce N-acetylaspartate (gray), or support purine and pyrimidine biosynthesis (orange). Aspartate fates that are affected by transaminase inhibition by AOA are indicated.

(B) Relative intracellular levels of NEAAs and TCA cycle intermediates in control (N) and AGC1-KD (A) C2C12 cells cultured in 0.1 mM glutamine (0.1 mM Q) or 4 mM glutamine with CB-839 for 24 hr in the presence and absence of 20 mM aspartate; relative change compared to control with CB-839 or NTC with 0.1 mM Q is shown (n = 3). Cit, citrate; a-KG, alpha-ketoglutarate; Suc, succinate; Fum, fumarate; Mal, malate; Asp, aspartate; Asn, asparagine; Gln, glutamine; Glu, glutamate; Pro, proline; Ser, serine; Gly, glycine; Ala, alanine.

(C) Proliferation/survival rates of control (NTC) and AGC1-KD C2C12 cells cultured in pyruvate-free DMEM and treated with 1 μM CB-839 in the presence or absence of 20 mM aspartate (Asp); 1 mM mixture of NEAAs containing serine, glycine, alanine, aspartate, asparagine, proline, and glutamate (NEAAs); and/or 0.3 mM AOA as indicated (n = 3).

(D) Proliferation/survival rates of control (NTC) and AGC1-KD C2C12 cells cultured in pyruvate-free DMEM and 0.1 mM mixture of NEAAs, and treated with 1 μM CB-839 in the presence or absence of 20 mM aspartate (Asp) and/or 0.3 mM AOA as indicated (n = 3).

(E) Proliferation/survival rates of control (NTC) and AGC1-KD C2C12 cells cultured in 4 mM glutamine and treated with DMSO or with 1 μM CB-839 in the presence of 10 mM aspartate (Asp); 1 mM of a mixture of NEAAs containing asparagine (Asn), serine (Ser), glycine (Gly), proline (Pro), alanine, aspartate (Asp), and glutamate (Glu) (NEAAs); or 1 mM of the individual specified free amino acid, as indicated (n = 3).

(F) Proliferation/survival rates of control (NTC) and AGC1-KD C2C12 cells cultured in 4 mM glutamine with 1 μM CB-839 and 0.1 mM mixture of NEAAs in the presence or absence of 20 mM aspartate (Asp), 2 mM dimethyl-α-ketoglutarate (daKG), and/or 0.3 mM AOA, as indicated (n = 3).

(G) Proliferation/survival rates of control (NTC) and AGC1-KD C2C12 cells treated with 1 μM CB-839 in the presence or absence of 20 mM aspartate (Asp), 2 mM dimethyl-α-ketoglutarate (daKG), and/or 2 mM sodium pyruvate (Pyr), without (siCtrl) or with (siGot1/2) siRNA KD of Got1 and Got2, as indicated (n = 3).

(H) Top: schematic showing the need for aspartate to make AMP from IMP. Bottom: relative AMP to IMP ratio in control (NTC) and AGC1-KD C2C12 cells cultured with 4 mM glutamine for 24 hr in the absence (Vehicle) or presence of 1 μM CB-839, without or with 20 mM aspartate (Asp), as indicated (n = 3).

(I) Top: schematic showing the role of aspartate in UMP synthesis. Bottom: relative intracellular UMP levels in control (NTC) and AGC1-KD C2C12 cells cultured in 4 mM glutamine for 24 hr in the absence (Vehicle) or presence of 1 μM CB-839, without or with 20 mM aspartate (Asp), as indicated (n = 3).

(J) Proliferation/survival rates of control (NTC) and AGC1-KD C2C12 cells cultured in 0.1 or 4 mM glutamine with 1 μM CB-839 in the presence or absence of a mix of nucleotide precursors containing 200 μM hypoxanthine, 200 μM adenine, 200 μM guanine, 100 μM thymine, and 400 μM uridine, as indicated (n = 3).

All figures denote mean ± SD unless indicated otherwise. *p ≤ 0.05, **p ≤ 0.01, ***p ≤ 0.001. See also Figure S5.

The finding that aspartate rescues proliferation/survival in the presence of AOA argues that aspartate contribution to the TCA cycle or to cytosolic NAD+ regeneration is not essential to rescue proliferation/survival when glutamine is limiting, as these aspartate functions involve transamination reactions (Figure S5D). Similar to NEAAs, neither daKG nor pyruvate can completely rescue glutamine limitation when aspartate aminotransferases are inhibited using AOA or small interfering RNA (siRNA) (Figures 6F, 6G, S5E, and S5F), suggesting that conversion of aspartate to oxaloacetate by transamination reactions either to regenerate cytosolic NAD+ or to donate nitrogen is not limiting in AGC1-KD cells upon glutamine deprivation. These data also argue that a major role of TCA cycle anaplerosis is to produce aspartate. However, it is important to note that these findings do not argue that aspartate does not undergo transamination and/or fuel the TCA cycle, but only suggest that these pathways are not limiting in low-glutamine conditions. In fact, we observed that [$U^{13}C$] aspartate is incorporated into TCA cycle intermediates in low-glutamine conditions (Figure S5H). Similarly, aspartate supplementation modestly increases some TCA cycle intermediates (Figure 6B), although these changes are inconsistent across different cell lines (Figures S4C and S4D). Notably, [$U^{13}C$]glutamate labels TCA cycle intermediates more than [$U^{13}C$]aspartate (Figure S5I), suggesting that even when transaminases are active, glutamate is a better TCA cycle fuel than aspartate (Figures S5H and S5I).

Another downstream fate of cytosolic aspartate that is not blocked by AOA is the synthesis of asparagine. Asparagine availability can affect cell survival following glutamine deprivation (Zhang et al., 2014), and intracellular asparagine acts as an exchange factor to import other extracellular amino acids when glutamine metabolism is compromised (Krall et al., 2016). Levels of asparagine are also reduced in AGC1-KD cells upon glutamine starvation, and these levels are partially recovered by aspartate supplementation (Figure 6B). However, asparagine supplementation, even at concentrations up to 10 mM, failed to rescue CB-839-treated AGC1-KD cells (Figures 6E and S5G), indicating that asparagine production by itself is not limiting for AGC1-KD cell survival following CB-839 treatment.

Aspartate is required for proliferation partly because it supports nucleotide biosynthesis (Sullivan et al., 2015). Glutaminase inhibition suppresses pyrimidine biosynthesis in Von Hippel-Lindau (VHL)-deficient renal tumors (Okazaki et al., 2017), suggesting that these perturbations might converge on nucleotide metabolism. When aspartate is used for purine biosynthesis, fumarate is generated as a byproduct (Lane and Fan, 2015). We considered that this may account for a greater increase in fumarate levels compared to other TCA cycle intermediates after aspartate supplementation (Figure 6B). To test whether glutaminase inhibition affects nucleotide biosynthesis, we traced [^{15}N-(amide)]glutamine into nucleotides following CB-839 treatment. Because aspartate donates its nitrogen to IMP for AMP production, AMP synthesis from IMP could be impaired when cytosolic aspartate is limiting (Figure S5J). Consistent with this, the relative AMP/IMP ratio is lower upon CB-839 treatment and is rescued by aspartate supplementation (Figure 6H), arguing that aspartate depletion slows nucleotide biosynthesis. Similarly, intracellular UMP levels are also lower in AGC1-KD cells upon CB-839 treatment compared to controls, suggesting that pyrimidine synthesis is also affected by decreased cytosolic aspartate delivery (Figure 6I). To test whether nucleotides were indeed limiting for AGC1-KD cells, we supplemented AGC1-KD and control cells with thymine, uridine, hypoxanthine, adenine, and guanine. These nucleotide bases improved AGC1-KD cell proliferation/survival in low-glutamine conditions or following glutaminase inhibition (Figures 6J and S5K), although this rescue was less prominent than that observed with aspartate. These data suggest that nucleotide biosynthesis is one limitation caused by decreased cytosolic aspartate delivery.

AGC1 Knockdown Limits Tumor Growth and Sensitizes Tumors to CB-839 Treatment

We next examined whether AGC1 KD would affect tumor growth *in vivo*. We injected LLC1 cells with or without AGC1-KD into syngeneic C57BL/6 mice and monitored tumor progression. KD of AGC1 slowed tumor growth over the course of 16 days (Figures S6A and S6B).

CB-839 is ineffective in limiting tumor growth in some cancer models *in vivo* even when the cells derived from those tumors are sensitive to CB-839 in culture (Biancur et al., 2017; Davidson et al., 2016). To test whether AGC1-KD sensitizes tumors to CB-839 *in vivo*, we exposed mice with control and AGC1-KD LLC1 tumors to CB-839. CB-839 treatment further reduced the growth of AGC1-KD LLC1 tumors (Figures 7A and S6C) while having a minor effect on control tumors, despite causing comparable drops in glutamate/glutamine ratio in both (Figure 7B). Similar to *in vitro* culture, pyruvate/lactate ratio was lower in AGC1-KD tumors, highlighting that loss of AGC1 also affects the redox state of cells *in vivo* (Figure 7C). Interestingly, asparagine levels were increased in CB-839 treated tumors, yet were lower in AGC1-KD tumors compared to controls (Figures 7D and S6D). These findings are consistent with mitochondrial aspartate export being important in tumors when glutaminase is inhibited and consistent with an inability to maintain cytosolic aspartate levels, slowing the growth of AGC1-KD tumors upon CB-839 treatment. These findings also argue that AGC1-KD increases tumor vulnerability to glutaminase inhibition.

To test whether AGC1-KD would have similar effects on another cancer type, we allografted AL1376 pancreatic ductal adenocarcinoma cells that were derived from the LSL-KrasG12D, $p53^{flox/flox}$, Pdx1-Cre mouse model (Bardeesy et al., 2006). Consistently, AGC1-KD significantly impaired tumor growth (Figure S6E). In addition, unlike LLC1, AL1376 tumors were completely resistant to CB-839 treatment, yet AGC1-KD promoted CB-839 sensitivity (Figures S6E and S6F). These data suggest that targeting AGC1 may synergize with the glutaminase inhibitors to limit the growth of some tumors.

Because AGC1-KD impaired *in vivo* growth of mouse lung and pancreas cancer cell lines, we checked whether autochthonous tumors also express AGC1 protein. Although AGC1 protein levels are not increased in either $Kras^{G12D}$, $p53^{-/-}$ mouse lung (Davidson et al., 2016) or pancreatic (Mayers et al., 2014) tumors that are resistant to CB-839 compared to corresponding healthy tissues, both tumor types had abundant AGC1 expression (Figure S7C). To explore the relevance of our findings in human cancer, we investigated AGC1 expression in several human solid tumors using immunohistochemistry with an antibody against AGC1. AGC1 is expressed in glioblastoma, as well as

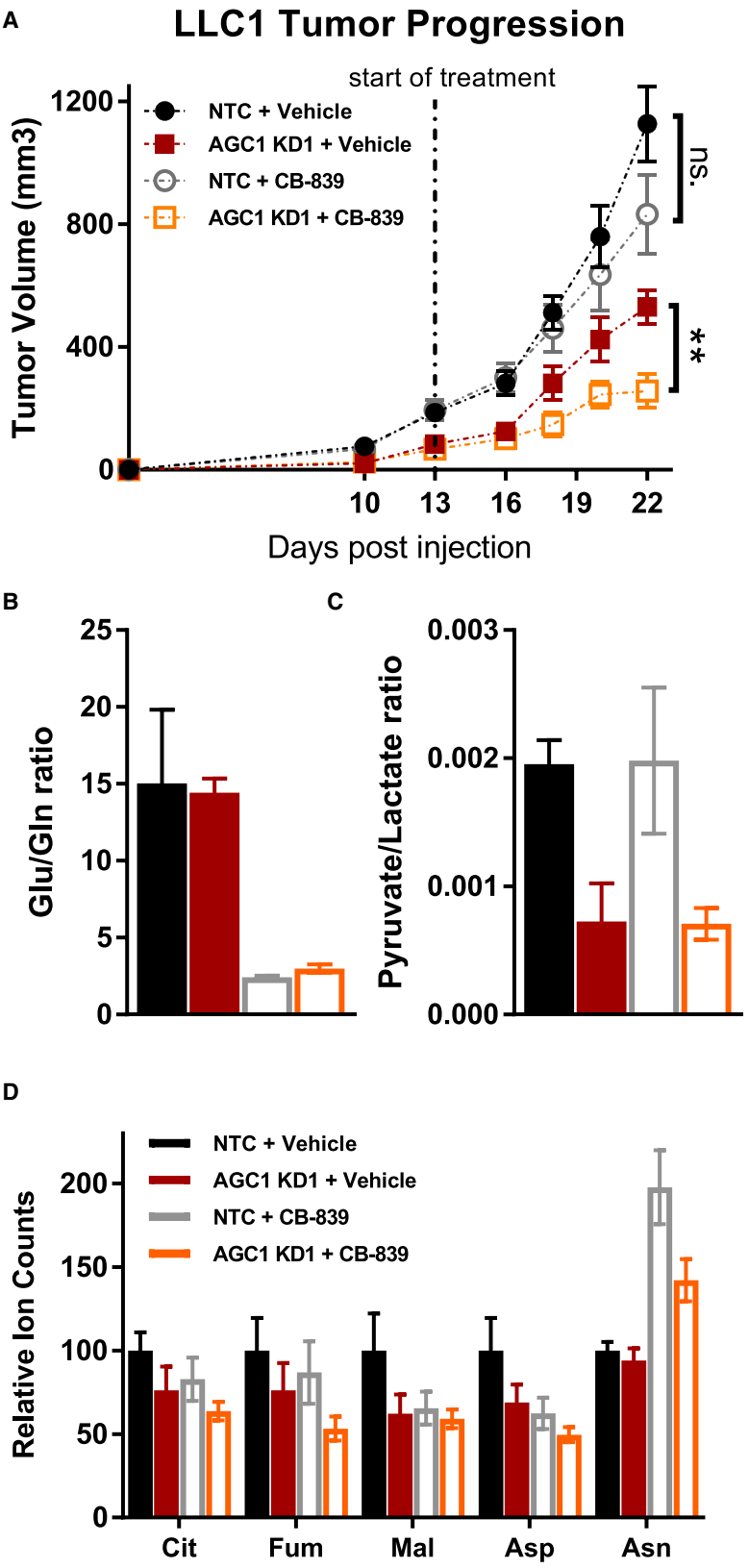

Figure 7. AGC1 Deficiency Sensitizes Tumors to CB-839 Treatment

(A) Growth of tumors generated from control (NTC) or AGC1-KD LLC1 in C56BL/6 mice flanks that were treated without (Vehicle) or with CB-839 dosed at 200 mg/kg twice daily starting on day 13 as indicated ($n \geq 6$).

(B) Relative glutamate (Glu) to glutamine (Gln) ratio measured in metabolite extracts from the tumors shown in (A) at the experimental endpoint (day 22) ($n \geq 5$).

(C) Relative pyruvate to lactate ratio measured in metabolite extracts from the tumors shown in (A) at the experimental endpoint (day 22) ($n \geq 5$).

(D) Relative levels of the specified TCA intermediates and asparagine (normalized to valine) measured in metabolite extracts from the tumors shown in (A) at the experimental endpoint ($n \geq 5$). Cit, citrate; Fum, fumarate; Mal, malate; Asp, aspartate; Asn, asparagine.

All figures denote mean ± SEM. *$p \leq 0.05$, **$p \leq 0.01$, ***$p \leq 0.001$. See also Figures S6 and S7.

adenocarcinoma of ovary and pancreas (Figures S7A and S7B). While pancreatic ductal carcinoma (PDAC) cells have heterogeneous AGC1 expression, all healthy pancreatic duct cells are AGC1 negative, suggesting that AGC1 might be upregulated during tumorigenesis in this cancer type (Figure S7B). These observations argue that AGC1 could be a target to treat human cancers.

DISCUSSION

These findings argue that glutamine anaplerosis is important to produce aspartate, and that decreased cytosolic aspartate levels can lead to cell death. These findings are consistent with recent data showing AGC1-deficient neuroblastoma cells proliferate slower in low-glutamine media (Profilo et al., 2017). From a mechanistic standpoint, it appears that one function of AGC1 is to sustain proliferation/survival of glutamine-deprived cells by providing aspartate to the cytosol. While aspartate may become limiting for nucleotide biosynthesis following glutamine depletion, different aspartate fates could be more limiting in other circumstances. It is important to note that if one fate of aspartate is rescued, more aspartate will be available for other pathways, making it difficult to definitively conclude that nucleotide synthesis is the only critical fate of aspartate, particularly when levels of other NEAAs or TCA cycle intermediates are indirectly affected when cytosolic aspartate is depleted. It is also impossible to rescue aspartate use for protein synthesis in the same way that aspartate use for nucleotides can be rescued by providing exogenous bases, and a role in protein synthesis may be equally important even in the cells examined in this study. Furthermore, AGC2 is structurally and functionally similar to AGC1 (Thangaratnarajah et al., 2014) and expressed at different levels in various tissues (Begum et al., 2002). Therefore, AGC2 depletion could be more harmful for some cell types than AGC1 depletion, and complete loss of both isoforms could cause more severe limitations to impair cell survival, perhaps even under glutamine-replete conditions.

Glutamine metabolism in cancer can be influenced by the environment (Davidson et al., 2016). For instance, supraphysiological cystine levels in tissue culture media can promote both glutaminase activity and glutamine dependency (Muir et al., 2017). Consistent with these findings, glutamine contributes very little to the oxidative TCA cycle in some cancers *in vivo* (Davidson et al., 2016). Similar to high-cystine conditions, increased mitochondrial NAD+/NADH ratio could also enhance oxidative glutamine metabolism and drive glutamine flux into aspartate synthesis. We observed that AGC1-KD suppressed reductive glutamine metabolism in C2C12 cells, and this may also be the case for LLC1 cells *in vivo*, potentially explaining why AGC1-KD tumors are sensitive to glutaminase inhibition *in vivo*.

There are three glutaminase isoforms in mammalian cells: liver isoform (LGA), kidney isoform (KGA), and a splice variant of KGA (GAC, also known as glutaminase C) that localizes to mitochondria (Cassago et al., 2012). GAC is the enzymatically most efficient isoform and is often upregulated in cancers, and connected to glutamine anaplerosis (Cassago et al., 2012). Upon CB-839 treatment, which selectively inhibits GAC (Gross et al., 2014), cells may utilize cytosolic glutamate as an alternative source. Because AGC1 exports aspartate from mitochondria in exchange for cytosolic glutamate, decreased glutamate delivery to mitochondria might also contribute to CB-839 toxicity in AGC1-KD cells. Decreased steady-state TCA cycle labeling from [U^{13}C]glutamate in AGC1-KD cells (Figure S5I) could suggest that mitochondrial glutamate entry might indeed be impaired. However, two other glutamate importers are located in the inner mitochondrial membrane, Slc25a22 and Slc25a18 (Palmieri, 2013), and these transporters may maintain some mitochondrial glutamate delivery in AGC1-KD cells. In support of this, the inability of α-KG to fully rescue glutamine limitation when aspartate synthesis is blocked suggests that a potential deficiency in mitochondrial glutamate uptake might be a factor that exacerbates the drop in mitochondrial aspartate levels in AGC1-KD cells.

Although low glutamine and CB-839 treatment lead to similar phenotypes, these two conditions are not identical. Because low glutamine levels will affect more pathways than CB-839 treatment, cell proliferation/survival and the depletion of some NEAAs and TCA intermediates were more pronounced in low glutamine. However, CB-839 synergizes with AGC1-KD similarly to low glutamine, suggesting that decreased TCA cycle anaplerosis is one reason why AGC1-KD cells are sensitive to glutamine withdrawal. Mitochondrial transporters can be promiscuous and transport multiple metabolites across membranes with varying binding efficiencies (Fiermonte et al., 2009; Gutiérrez-Aguilar and Baines, 2013). For instance, uncoupling protein 2 (UCP2) can export four carbon metabolites from mitochondria, including aspartate (Vozza et al., 2014). We speculate that various mitochondrial transporters, including AGC2, maintain some degree of cytosolic aspartate delivery in AGC1-KD cells as long as aspartate levels in mitochondria are sufficiently high. Interestingly, not all anaplerotic substrates rescue glutamine limitation in AGC1-KD cells. Dimethlymalate (dMal, a cell-permeable form of malate) failed to rescue low glutamine or CB-839 treatment (Figure 5C), was unable to increase aspartate levels (Figures S4A and S4B), and caused a reduction in TCA intermediates in some conditions. These data suggest that dMal might have potentially harmful effects on cells other than solely supplying four carbon units to the TCA cycle.

We used asparagine levels as a proxy for cytosolic aspartate in cell culture experiments; however, the fact that mouse plasma contains asparagine (Rivera et al., 1987) may explain why asparagine levels are unchanged in AGC1-KD tumors compared to controls *in vivo*. Interestingly, asparagine levels were increased with CB-839 treatment *in vivo* independently of AGC1 expression, in line with recent reports pointing out that asparagine synthase expression is upregulated in CB-839-resistant cells (Biancur et al., 2017). This may suggest an independent, anti-apoptotic function for asparagine as previously reported (Zhang et al., 2014). In our system, asparagine supplementation had no effect on CB-839-treated cells *in vitro*; however, this may change when cells are adapted to grow in the presence of glutaminase inhibitors (Krall et al., 2016). In addition, because asparagine is produced from both cytosolic aspartate and glutamine, in media where glutamine is limited, asparagine levels may not be a good proxy for cytosolic aspartate and could explain why aspartate supplementation did not increase asparagine levels in low glutamine.

Aspartate availability can be limiting for tumor growth *in vivo* (Gui et al., 2016; Sullivan et al., 2018) and we find that AGC1 deficiency leads to both reduced cytosolic aspartate and increased dependence on glutaminase. Adaptive programs downstream of

glutamine withdrawal can also promote the uptake of extracellular aspartate (Tajan et al., 2018). These findings suggest that combination therapies targeting both aspartate and glutamine metabolism may be synergistic. We found that AGC1 plays a central role in sustaining cytosolic aspartate levels, particularly when mitochondrial glutaminolysis is compromised. This implies that targeting AGC1 could sensitize some cancers to glutaminase inhibitors. It is worth noting that genetic background and tissue of origin are also important aspects to consider for targeting metabolism (Mayers et al., 2016; Yuneva et al., 2012), and additional studies are necessary to define the cancer subsets that are most likely to respond to these interventions.

Environmental nutrients can also impact cancer cell metabolism (Tardito et al., 2015; Cantor et al., 2017; Muir et al., 2017; Muir and Vander Heiden, 2018). Another caveat of our study in this respect is that the mechanistic analysis for why cells require mitochondrial aspartate export used cells in culture that rely on glutamine for TCA cycle anaplerosis. However, glutamine is not the major source of aspartate for all tumor cells *in vivo* (Davidson et al., 2016; Muir et al., 2017), and some tumors have been shown to synthesize glutamine from glucose in a series of reactions that consume TCA cycle intermediates (Tardito et al., 2015; Hensley et al., 2016). Thus, despite showing that AGC1 loss can sensitize some tumors to glutaminase inhibition, whether tumors that use the TCA cycle to make, rather than consume, glutamine exhibit a similar dependence on AGC1 remains unknown. Furthermore, potential toxicities of AGC inhibition in healthy cells could limit targeting of AGC1, as AGC1 deficiency in mice and humans leads to loss of motor coordination and neuronal defects (Falk et al., 2014; Jalil et al., 2005; Sakurai et al., 2010; Wibom et al., 2009), while loss-of-function mutations in AGC2 lead to the urea cycle-associated disorder type II citrullinemia (Saheki et al., 2002; Yasuda et al., 2000). Nevertheless, our data provide evidence that in some contexts tumor-specific inhibition of AGC1 can reduce tumor growth, and this effect can be exacerbated by glutaminase inhibition.

STAR★METHODS

Detailed methods are provided in the online version of this paper and include the following:

- KEY RESOURCES TABLE
- CONTACT FOR REAGENT AND RESOURCE SHARING
- EXPERIMENTAL MODEL AND SUBJECT DETAILS
  - Cell Lines
  - Animals
- METHOD DETAILS
  - Stable-knockdown of AGC1
  - Proliferation/Survival Rates
  - Cell Viability Assays
  - Determining Annexin V/Propidium Iodide staining using flow cytometry
  - Transient overexpression of mouse and human AGC1
  - CRISPR/Cas9-mediated knock-out of AGC1
  - siRNA-mediated knock-down of Got1/2
  - NAD+/NADH Measurements
  - Mitochondrial Oxygen Consumption
  - Isotope Tracing and GCMS Analysis
  - Metabolic profiling using LCMS
  - Metabolite Measurements using NMR
  - Immunohistochemistry
  - Radioactive CO_2 Release
  - Extracellular Flux Analysis
  - Western blot analysis
  - Quantitative Real-Time PCR
- QUANTIFICATION AND STATISTICAL ANALYSIS

SUPPLEMENTAL INFORMATION

Supplemental Information includes seven figures and can be found with this article online at https://doi.org/10.1016/j.cmet.2018.07.021.

ACKNOWLEDGMENTS

This work was funded by the Austrian Science Fund FWF SFB LIPTOX F3018, P27108, P28854, W1226 DK "Metabolic and Cardiovascular Disease," the Integrative Metabolism Research Center Graz, and the Austrian infrastructure program 2016/2017. M.G.V.H. acknowledges support from the Lustgarten Foundation, SU2C, the Ludwig Center at MIT, the MIT Center for Precision Cancer Medicine, and the NCI (P30 CA1405141 and R01 CA168653). M.G.V.H. is also an HHMI faculty scholar. H.F.A. was supported by Austrian Marshall Plan Scholarship. A.L. is supported by the Ludwig Center for Molecular Oncology Fund, NSF (GRFP DGE-1122374), and T32GM007287. S.S. was trained within frame of the PhD program Molecular Medicine. A.N.L. is a Robert Black Fellow of the Damon Runyon Cancer Research Foundation, DRG-2241-15. W.A.-Z. is supported by CBmed – Center for Biomarker Research in Medicine. We thank Thales Papagiannakopoulos for sharing CB-839. We are grateful for all the people in the Vander Heiden and Bogner-Strauss labs, especially Aaron Hosios, Lucas Sullivan, Zhaoqi Li, Laura Danai, Ariane Pessentheiner, and Daniel Schmidt, for constructive discussions, experimental advice, and critical reading of the manuscript. We acknowledge the support of NAWI Graz and the technical support of Thomas Schreiner, Wolfgang Krispel, Silvia Schauer, and Bena Chan.

AUTHOR CONTRIBUTIONS

H.F.A. designed and performed the majority of the experiments. K.E.W. and A.L. assisted with some *in vitro* and *in vivo* experiments, respectively. C.T.M.-S. and W.F.G. determined oxygen consumption. S.S. and T.M. performed NMR measurements and data analysis. A.N.L. assisted with flow cytometry experiments and generated the AL1376 cell line. W.A.-Z. and G.H. assessed immunohistochemistry slides. C.A.L. performed liquid chromatography-mass spectrometry measurements. C.J.T. supplied critical reagents. H.F.A. and J.G.B.-S. constructed the study and M.G.V.H. provided substantial guidance and shared lab space and equipment. H.F.A., M.G.V.H., and J.G.B.-S. wrote the manuscript.

DECLARATION OF INTERESTS

M.G.V.H. discloses that he is a consultant and scientific advisory board member for Agios Pharmaceuticals and Aeglea Biotherapeutics, and T.M. discloses that he is a consultant and scientific advisory board member of Cleara Biotech.

Received: August 17, 2017
Revised: May 29, 2018
Accepted: July 29, 2018
Published: August 16, 2018

REFERENCES

Ahn, C.S., and Metallo, C.M. (2015). Mitochondria as biosynthetic factories for cancer proliferation. Cancer Metab. *3*, 1.

Amoedo, N.D., Punzi, G., Obre, E., Lacombe, D., De Grassi, A., Pierri, C.L., and Rossignol, R. (2016). AGC1/2, the mitochondrial aspartate-glutamate carriers. Biochim. Biophys. Acta *1863*, 2394–2412.

Bardeesy, N., Aguirre, A.J., Chu, G.C., Cheng, K.H., Lopez, L.V., Hezel, A.F., Feng, B., Brennan, C., Weissleder, R., Mahmood, U., et al. (2006). Both p16(Ink4a) and the p19(Arf)-p53 pathway constrain progression of pancreatic adenocarcinoma in the mouse. Proc. Natl. Acad. Sci. USA *103*, 5947–5952.

Begum, L., Jalil, M.A., Kobayashi, K., Iijima, M., Li, M.X., Yasuda, T., Horiuchi, M., del Arco, A., Satrústegui, J., and Saheki, T. (2002). Expression of three mitochondrial solute carriers, citrin, aralar1 and ornithine transporter, in relation to urea cycle in mice. Biochim. Biophys. Acta *1574*, 283–292.

Biancur, D.E., Paulo, J.A., Małachowska, B., Quiles Del Rey, M., Sousa, C.M., Wang, X., Sohn, A.S.W., Chu, G.C., Gygi, S.P., Harper, J.W., et al. (2017). Compensatory metabolic networks in pancreatic cancers upon perturbation of glutamine metabolism. Nat. Commun. *8*, 15965.

Birsoy, K., Wang, T., Chen, W.W., Freinkman, E., Abu-Remaileh, M., and Sabatini, D.M. (2015). An essential role of the mitochondrial electron transport chain in cell proliferation is to enable aspartate synthesis. Cell *162*, 540–551.

Bogner-Strauss, J.G. (2017). *N*-Acetylaspartate metabolism outside the brain: lipogenesis, histone acetylation, and cancer. Front. Endocrinol. (Lausanne) *8*, 240.

Cantor, J.R., and Sabatini, D.M. (2012). Cancer cell metabolism: one hallmark, many faces. Cancer Discov. *2*, 881–898.

Cantor, J.R., Abu-Remaileh, M., Kanarek, N., Freinkman, E., Gao, X., Louissaint, A., Jr., Lewis, C.A., and Sabatini, D.M. (2017). Physiologic medium rewires cellular metabolism and reveals uric acid as an endogenous inhibitor of UMP synthase. Cell *169*, 258–272.e17.

Cassago, A., Ferreira, A.P., Ferreira, I.M., Fornezari, C., Gomes, E.R., Greene, K.S., Pereira, H.M., Garratt, R.C., Dias, S.M., and Ambrosio, A.L. (2012). Mitochondrial localization and structure-based phosphate activation mechanism of Glutaminase C with implications for cancer metabolism. Proc. Natl. Acad. Sci. USA *109*, 1092–1097.

Catalina-Rodriguez, O., Kolukula, V.K., Tomita, Y., Preet, A., Palmieri, F., Wellstein, A., Byers, S., Giaccia, A.J., Glasgow, E., Albanese, C., and Avantaggiati, M.L. (2012). The mitochondrial citrate transporter, CIC, is essential for mitochondrial homeostasis. Oncotarget *3*, 1220–1235.

Chen, R., Zou, Y., Mao, D., Sun, D., Gao, G., Shi, J., Liu, X., Zhu, C., Yang, M., Ye, W., et al. (2014). The general amino acid control pathway regulates mTOR and autophagy during serum/glutamine starvation. J. Cell Biol. *206*, 173–182.

Christensen, C.E., Karlsson, M., Winther, J.R., Jensen, P.R., and Lerche, M.H. (2014). Non-invasive in-cell determination of free cytosolic [NAD+]/[NADH] ratios using hyperpolarized glucose show large variations in metabolic phenotypes. J. Biol. Chem. *289*, 2344–2352.

Cory, J.G., and Cory, A.H. (2006). Critical roles of glutamine as nitrogen donors in purine and pyrimidine nucleotide synthesis: asparaginase treatment in childhood acute lymphoblastic leukemia. In Vivo *20*, 587–589.

Davidson, S.M., Papagiannakopoulos, T., Olenchock, B.A., Heyman, J.E., Keibler, M.A., Luengo, A., Bauer, M.R., Jha, A.K., O'Brien, J.P., Pierce, K.A., et al. (2016). Environment impacts the metabolic dependencies of Ras-driven non-small cell lung cancer. Cell Metab. *23*, 517–528.

DeBerardinis, R.J., and Chandel, N.S. (2016). Fundamentals of cancer metabolism. Sci. Adv. *2*, e1600200.

del Arco, A., Morcillo, J., Martínez-Morales, J.R., Galián, C., Martos, V., Bovolenta, P., and Satrústegui, J. (2002). Expression of the aspartate/glutamate mitochondrial carriers aralar1 and citrin during development and in adult rat tissues. Eur. J. Biochem. *269*, 3313–3320.

Dixon, S.J., Patel, D.N., Welsch, M., Skouta, R., Lee, E.D., Hayano, M., Thomas, A.G., Gleason, C.E., Tatonetti, N.P., Slusher, B.S., and Stockwell, B.R. (2014). Pharmacological inhibition of cystine-glutamate exchange induces endoplasmic reticulum stress and ferroptosis. eLife *3*, e02523.

Falk, M.J., Li, D., Gai, X., McCormick, E., Place, E., Lasorsa, F.M., Otieno, F.G., Hou, C., Kim, C.E., Abdel-Magid, N., et al. (2014). AGC1 deficiency causes infantile epilepsy, abnormal myelination, and reduced N-acetylaspartate. JIMD Rep. *14*, 77–85.

Fernandez, C.A., Des Rosiers, C., Previs, S.F., David, F., and Brunengraber, H. (1996). Correction of 13C mass isotopomer distributions for natural stable isotope abundance. J. Mass Spectrom. *31*, 255–262.

Fiermonte, G., Paradies, E., Todisco, S., Marobbio, C.M., and Palmieri, F. (2009). A novel member of solute carrier family 25 (SLC25A42) is a transporter of coenzyme A and adenosine 3′,5′-diphosphate in human mitochondria. J. Biol. Chem. *284*, 18152–18159.

Greenhouse, W.V., and Lehninger, A.L. (1976). Occurrence of the malate-aspartate shuttle in various tumor types. Cancer Res. *36*, 1392–1396.

Gross, M.I., Demo, S.D., Dennison, J.B., Chen, L., Chernov-Rogan, T., Goyal, B., Janes, J.R., Laidig, G.J., Lewis, E.R., Li, J., et al. (2014). Antitumor activity of the glutaminase inhibitor CB-839 in triple-negative breast cancer. Mol. Cancer Ther. *13*, 890–901.

Gui, D.Y., Sullivan, L.B., Luengo, A., Hosios, A.M., Bush, L.N., Gitego, N., Davidson, S.M., Freinkman, E., Thomas, C.J., and Vander Heiden, M.G. (2016). Environment dictates dependence on mitochondrial complex I for NAD+ and aspartate production and determines cancer cell sensitivity to metformin. Cell Metab. *24*, 716–727.

Gutiérrez-Aguilar, M., and Baines, C.P. (2013). Physiological and pathological roles of mitochondrial SLC25 carriers. Biochem. J. *454*, 371–386.

Hensley, C.T., Faubert, B., Yuan, Q., Lev-Cohain, N., Jin, E., Kim, J., Jiang, L., Ko, B., Skelton, R., Loudat, L., et al. (2016). Metabolic heterogeneity in human lung tumors. Cell *164*, 681–694.

Hosios, A.M., Hecht, V.C., Danai, L.V., Johnson, M.O., Rathmell, J.C., Steinhauser, M.L., Manalis, S.R., and Vander Heiden, M.G. (2016). Amino acids rather than glucose account for the majority of cell mass in proliferating mammalian cells. Dev. Cell *36*, 540–549.

Jalil, M.A., Begum, L., Contreras, L., Pardo, B., Iijima, M., Li, M.X., Ramos, M., Marmol, P., Horiuchi, M., Shimotsu, K., et al. (2005). Reduced N-acetylaspartate levels in mice lacking aralar, a brain- and muscle-type mitochondrial aspartate-glutamate carrier. J. Biol. Chem. *280*, 31333–31339.

Jiang, L., Boufersaoui, A., Yang, C., Ko, B., Rakheja, D., Guevara, G., Hu, Z., and DeBerardinis, R.J. (2017). Quantitative metabolic flux analysis reveals an unconventional pathway of fatty acid synthesis in cancer cells deficient for the mitochondrial citrate transport protein. Metab. Eng. *43* (Pt B), 198–207.

Krall, A.S., Xu, S., Graeber, T.G., Braas, D., and Christofk, H.R. (2016). Asparagine promotes cancer cell proliferation through use as an amino acid exchange factor. Nat. Commun. *7*, 11457.

Lane, A.N., and Fan, T.W. (2015). Regulation of mammalian nucleotide metabolism and biosynthesis. Nucleic Acids Res. *43*, 2466–2485.

Lewis, C.A., Parker, S.J., Fiske, B.P., McCloskey, D., Gui, D.Y., Green, C.R., Vokes, N.I., Feist, A.M., Vander Heiden, M.G., and Metallo, C.M. (2014). Tracing compartmentalized NADPH metabolism in the cytosol and mitochondria of mammalian cells. Mol. Cell *55*, 253–263.

Lou, T.F., Sethuraman, D., Dospoy, P., Srivastva, P., Kim, H.S., Kim, J., Ma, X., Chen, P.H., Huffman, K.E., Frink, R.E., et al. (2016). Cancer-specific production of N-acetylaspartate via NAT8L overexpression in non-small cell lung cancer and its potential as a circulating biomarker. Cancer Prev. Res. (Phila.) *9*, 43–52.

Lunt, S.Y., and Vander Heiden, M.G. (2011). Aerobic glycolysis: meeting the metabolic requirements of cell proliferation. Annu. Rev. Cell Dev. Biol. *27*, 441–464.

Mayers, J.R., Wu, C., Clish, C.B., Kraft, P., Torrence, M.E., Fiske, B.P., Yuan, C., Bao, Y., Townsend, M.K., Tworoger, S.S., et al. (2014). Elevation of circulating branched-chain amino acids is an early event in human pancreatic adenocarcinoma development. Nat. Med. *20*, 1193–1198.

Mayers, J.R., Torrence, M.E., Danai, L.V., Papagiannakopoulos, T., Davidson, S.M., Bauer, M.R., Lau, A.N., Ji, B.W., Dixit, P.D., Hosios, A.M., et al. (2016). Tissue of origin dictates branched-chain amino acid metabolism in mutant Kras-driven cancers. Science *353*, 1161–1165.

Metallo, C.M., Gameiro, P.A., Bell, E.L., Mattaini, K.R., Yang, J., Hiller, K., Jewell, C.M., Johnson, Z.R., Irvine, D.J., Guarente, L., et al. (2011). Reductive glutamine metabolism by IDH1 mediates lipogenesis under hypoxia. Nature *481*, 380–384.

Muir, A., and Vander Heiden, M.G. (2018). The nutrient environment affects therapy. Science *360*, 962–963.

Muir, A., Danai, L.V., Gui, D.Y., Waingarten, C.Y., Lewis, C.A., and Vander Heiden, M.G. (2017). Environmental cystine drives glutamine anaplerosis

and sensitizes cancer cells to glutaminase inhibition. eLife *6*, e27713, https://doi.org/10.7554/eLife.27713.

Mullen, A.R., Wheaton, W.W., Jin, E.S., Chen, P.H., Sullivan, L.B., Cheng, T., Yang, Y., Linehan, W.M., Chandel, N.S., and DeBerardinis, R.J. (2011). Reductive carboxylation supports growth in tumour cells with defective mitochondria. Nature *481*, 385–388.

Mullen, A.R., Hu, Z., Shi, X., Jiang, L., Boroughs, L.K., Kovacs, Z., Boriack, R., Rakheja, D., Sullivan, L.B., Linehan, W.M., et al. (2014). Oxidation of alpha-ketoglutarate is required for reductive carboxylation in cancer cells with mitochondrial defects. Cell Rep. *7*, 1679–1690.

Okazaki, A., Gameiro, P.A., Christodoulou, D., Laviollette, L., Schneider, M., Chaves, F., Stemmer-Rachamimov, A., Yazinski, S.A., Lee, R., Stephanopoulos, G., et al. (2017). Glutaminase and poly(ADP-ribose) polymerase inhibitors suppress pyrimidine synthesis and VHL-deficient renal cancers. J. Clin. Invest. *127*, 1631–1645.

Palmieri, F. (2013). The mitochondrial transporter family SLC25: identification, properties and physiopathology. Mol. Aspects Med. *34*, 465–484.

Palmieri, L., Pardo, B., Lasorsa, F.M., del Arco, A., Kobayashi, K., Iijima, M., Runswick, M.J., Walker, J.E., Saheki, T., Satrústegui, J., and Palmieri, F. (2001). Citrin and aralar1 are Ca(2+)-stimulated aspartate/glutamate transporters in mitochondria. EMBO J. *20*, 5060–5069.

Pochini, L., Scalise, M., Galluccio, M., and Indiveri, C. (2014). Membrane transporters for the special amino acid glutamine: structure/function relationships and relevance to human health. Front Chem. *2*, 61.

Profilo, E., Peña-Altamira, L.E., Corricelli, M., Castegna, A., Danese, A., Agrimi, G., Petralla, S., Giannuzzi, G., Porcelli, V., Sbano, L., et al. (2017). Down-regulation of the mitochondrial aspartate-glutamate carrier isoform 1 AGC1 inhibits proliferation and N-acetylaspartate synthesis in Neuro2A cells. Biochim. Biophys. Acta *1863*, 1422–1435.

Prokesch, A., Graef, F.A., Madl, T., Kahlhofer, J., Heidenreich, S., Schumann, A., Moyschewitz, E., Pristoynik, P., Blaschitz, A., Knauer, M., et al. (2017). Liver p53 is stabilized upon starvation and required for amino acid catabolism and gluconeogenesis. FASEB J. *31*, 732–742.

Radović, B., Vujić, N., Leopold, C., Schlager, S., Goeritzer, M., Patankar, J.V., Korbelius, M., Kolb, D., Reindl, J., Wegscheider, M., et al. (2016). Lysosomal acid lipase regulates VLDL synthesis and insulin sensitivity in mice. Diabetologia *59*, 1743–1752.

Rivera, S., López-Soriano, F.J., Azcón-Bieto, J., and Argilés, J.M. (1987). Blood amino acid compartmentation in mice bearing Lewis lung carcinoma. Cancer Res. *47*, 5644–5646.

Rubi, B., del Arco, A., Bartley, C., Satrustegui, J., and Maechler, P. (2004). The malate-aspartate NADH shuttle member Aralar1 determines glucose metabolic fate, mitochondrial activity, and insulin secretion in beta cells. J. Biol. Chem. *279*, 55659–55666.

Saheki, T., Kobayashi, K., Iijima, M., Nishi, I., Yasuda, T., Yamaguchi, N., Gao, H.Z., Jalil, M.A., Begum, L., and Li, M.X. (2002). Pathogenesis and pathophysiology of citrin (a mitochondrial aspartate glutamate carrier) deficiency. Metab. Brain Dis. *17*, 335–346.

Sakurai, T., Ramoz, N., Barreto, M., Gazdoiu, M., Takahashi, N., Gertner, M., Dorr, N., Gama Sosa, M.A., De Gasperi, R., Perez, G., et al. (2010). Slc25a12 disruption alters myelination and neurofilaments: a model for a hypomyelination syndrome and childhood neurodevelopmental disorders. Biol. Psychiatry *67*, 887–894.

Sanjana, N.E., Shalem, O., and Zhang, F. (2014). Improved vectors and genome-wide libraries for CRISPR screening. Nat. Methods *11*, 783–784.

Shalem, O., Sanjana, N.E., Hartenian, E., Shi, X., Scott, D.A., Mikkelson, T., Heckl, D., Ebert, B.L., Root, D.E., Doench, J.G., and Zhang, F. (2014). Genome-scale CRISPR-Cas9 knockout screening in human cells. Science *343*, 84–87.

Sullivan, L.B., Gui, D.Y., Hosios, A.M., Bush, L.N., Freinkman, E., and Vander Heiden, M.G. (2015). Supporting aspartate biosynthesis is an essential function of respiration in proliferating cells. Cell *162*, 552–563.

Sullivan, L.B., Luengo, A., Danai, L.V., Bush, L.N., Diehl, F.F., Hosios, A.M., Lau, A.N., Elmiligy, S., Malstrom, S., Lewis, C.A., and Vander Heiden, M.G. (2018). Aspartate is an endogenous metabolic limitation for tumour growth. Nat. Cell Biol. *20*, 782–788.

Tajan, M., Hock, A.K., Blagih, J., Robertson, N.A., Labuschagne, C.F., Kruiswijk, F., Humpton, T.J., Adams, P.D., and Vousden, K.H. (2018). A role for p53 in the adaptation to glutamine starvation through the expression of SLC1A3. Cell Metab. Published online August 16, 2018. https://doi.org/10.1016/j.cmet.2018.07.005.

Tardito, S., Oudin, A., Ahmed, S.U., Fack, F., Keunen, O., Zheng, L., Miletic, H., Sakariassen, P.Ø., Weinstock, A., Wagner, A., et al. (2015). Glutamine synthetase activity fuels nucleotide biosynthesis and supports growth of glutamine-restricted glioblastoma. Nat. Cell Biol. *17*, 1556–1568.

Thangaratnarajah, C., Ruprecht, J.J., and Kunji, E.R. (2014). Calcium-induced conformational changes of the regulatory domain of human mitochondrial aspartate/glutamate carriers. Nat. Commun. *5*, 5491.

Vander Heiden, M.G., and DeBerardinis, R.J. (2017). Understanding the intersections between metabolism and cancer biology. Cell *168*, 657–669.

Vander Heiden, M.G., Cantley, L.C., and Thompson, C.B. (2009). Understanding the Warburg effect: the metabolic requirements of cell proliferation. Science *324*, 1029–1033.

Vozza, A., Parisi, G., De Leonardis, F., Lasorsa, F.M., Castegna, A., Amorese, D., Marmo, R., Calcagnile, V.M., Palmieri, L., Ricquier, D., et al. (2014). UCP2 transports C4 metabolites out of mitochondria, regulating glucose and glutamine oxidation. Proc. Natl. Acad. Sci. USA *111*, 960–965.

Vyas, S., Zaganjor, E., and Haigis, M.C. (2016). Mitochondria and Cancer. Cell *166*, 555–566.

Warburg, O. (1956). On the origin of cancer cells. Science *123*, 309–314.

Wibom, R., Lasorsa, F.M., Töhönen, V., Barbaro, M., Sterky, F.H., Kucinski, T., Naess, K., Jonsson, M., Pierri, C.L., Palmieri, F., and Wedell, A. (2009). AGC1 deficiency associated with global cerebral hypomyelination. N. Engl. J. Med. *361*, 489–495.

Wiechert, W. (2007). The thermodynamic meaning of metabolic exchange fluxes. Biophys. J. *93*, 2255–2264.

Williamson, D.H., Lund, P., and Krebs, H.A. (1967). The redox state of free nicotinamide-adenine dinucleotide in the cytoplasm and mitochondria of rat liver. Biochem. J. *103*, 514–527.

Wise, D.R., and Thompson, C.B. (2010). Glutamine addiction: a new therapeutic target in cancer. Trends Biochem. Sci. *35*, 427–433.

Yasuda, T., Yamaguchi, N., Kobayashi, K., Nishi, I., Horinouchi, H., Jalil, M.A., Li, M.X., Ushikai, M., Iijima, M., Kondo, I., and Saheki, T. (2000). Identification of two novel mutations in the SLC25A13 gene and detection of seven mutations in 102 patients with adult-onset type II citrullinemia. Hum. Genet. *107*, 537–545.

Yuneva, M., Zamboni, N., Oefner, P., Sachidanandam, R., and Lazebnik, Y. (2007). Deficiency in glutamine but not glucose induces MYC-dependent apoptosis in human cells. J. Cell Biol. *178*, 93–105.

Yuneva, M.O., Fan, T.W., Allen, T.D., Higashi, R.M., Ferraris, D.V., Tsukamoto, T., Matés, J.M., Alonso, F.J., Wang, C., Seo, Y., et al. (2012). The metabolic profile of tumors depends on both the responsible genetic lesion and tissue type. Cell Metab. *15*, 157–170.

Zand, B., Previs, R.A., Zacharias, N.M., Rupaimoole, R., Mitamura, T., Nagaraja, A.S., Guindani, M., Dalton, H.J., Yang, L., Baddour, J., et al. (2016). Role of increased n-acetylaspartate levels in cancer. J. Natl. Cancer Inst. *108*, djv426.

Zhang, J., Fan, J., Venneti, S., Cross, J.R., Takagi, T., Bhinder, B., Djaballah, H., Kanai, M., Cheng, E.H., Judkins, A.R., et al. (2014). Asparagine plays a critical role in regulating cellular adaptation to glutamine depletion. Mol. Cell *56*, 205–218.

Zong, W.X., Rabinowitz, J.D., and White, E. (2016). Mitochondria and Cancer. Mol. Cell *61*, 667–676.

STAR★METHODS

KEY RESOURCES TABLE

REAGENT or RESOURCE	SOURCE	IDENTIFIER
Antibodies		
Mouse monoclonal α-Aralar (AGC1) antibody B2	Santa Cruz Biotechnology	Cat#: sc-271056; RRID: AB_10608837
Mouse monoclonal α-Beta actin antibody	Sigma-Aldrich	Cat#: A5316; RRID: AB_476743
Anti-mouse secondary antibody	Dako Österreich GmbH	Cat#: P0260; RRID: AB_2636929
Chemicals, Peptides, and Recombinant Proteins		
2-deoxyglucose	Sigma-Aldrich	Cat#: D8375-1G
D-Glucose > 99,5%, CELLPURE	Carl Roth GmbH	Art.-Nr. HN06.3
L-Glutamine	Sigma-Aldrich	Cat#: G6392-10VL
MEM 50X Amino Acid Solution	Sigma-Aldrich	Cat#: M5550
100X Non-essential Amino Acid Solution	Sigma-Aldrich	Cat#: M7145-100mL
Metformin	Sigma-Aldrich	Cat#: PHR1084-500MG
Sodium pyruvate	Sigma-Aldrich	Cat#: P2256-5G
dimethylalpha-ketoglutarate	Sigma-Aldrich	Cat#: 349631-5G
dimethylmalate	Sigma-Aldrich	Cat#: 238198-100G
L-Aspartate	Sigma-Aldrich	Cat#: A7219-100G
L-Asparagine monohydrate	Sigma-Aldrich	Cat#: A8381-100G
L-Glutamate	Sigma-Aldrich	Cat#: G1251-100G
L-Serine	Sigma-Aldrich	Cat#: S54500-1G
L-Glycine	Sigma-Aldrich	Cat#: G8790-100G
L-Alanine	Sigma-Aldrich	Cat#: A7627-1G
L-Proline	Sigma-Aldrich	Cat#: P5607
[^{13}C-U]-D-Glucose	Cambridge Isotopes Laboratories	Cat#: CLM-1396
[^{13}C-U]-L-Glutamine	Cambridge Isotopes Laboratories	Cat#: CLM-1822-H
[^{13}C-U]-L-Aspartate	Cambridge Isotopes Laboratories	Cat#: CLM-1801-H
[^{13}C-U]-L-Glutamate	Cambridge Isotopes Laboratories	Cat#: CLM-3949-PK
[U-14C]-glutamine	American Radiolabeled Chemicals	Cat#: ARC 0196
Adenine	Sigma-Aldrich	Cat#: A8626-5G
Guanine	Sigma-Aldrich	Cat#: G11950-10G
Hypoxanthine	Sigma-Aldrich	Cat#: H9377-5G
Thymine	Sigma-Aldrich	Cat#: T0376-5G
Uridine	Sigma-Aldrich	Cat#: U6381-5G
O-(Carboxymethyl)hydroxylamine hemihydrochloride (AOA)	N/A	Cat#: C13408-1G
Critical Commercial Assays		
Cell Titer Glo	Promega	Cat #: G7570
NAD/NADH Glo	Promega	Cat #: G9071
Dead Cell Apoptosis Kit	Thermo Fisher	Cat #: V13242
Deposited Data		
Cancer Cell Line Encyclopedia	Broad Institute	https://portals.broadinstitute.org/ccle
Experimental Models: Cell Lines		
Mouse: C2C12	ATCC	CRL-1772
Muse: LLC1	ATCC	CRL-1642
Mouse: AI1376	Our laboratory	N/A
Human: HeLa	ATCC	CCL-2
Human: A549	ATCC	CCL-185

(*Continued on next page*)

Continued		
REAGENT or RESOURCE	SOURCE	IDENTIFIER
Human: NCI-H1299	ATCC	CRL-5803
Human: PANC1	ATCC	CRL-1469
Human: CAPAN2	ATCC	HTB-80
Experimental Models: Organisms/Strains		
C57BL/6	Jackson Laboratories & Janvier	Stock No: 000664
Oligonucleotides		
mSlc25a12_guide 1:GCCATGCTGTGCTCGGAAGC	IDT DNA	custom oligo
mSlc25a12_guide 2:CCATGCTGTGCTCGGAAGCC	IDT DNA	custom oligo
mSlc25a12_guide 3:CTCATGAGGATCACCTCGTT	IDT DNA	custom oligo
mSlc25a12_guide 4:CAGGTGCATACAACCAAACG	IDT DNA	custom oligo
mSlc25a12_guide 5:GGCTTCCGAGCACAGCATGG	IDT DNA	custom oligo
mSlc25a12_guide 6:ACTCGCAGTCCCAGTTAAAA	IDT DNA	custom oligo
mSlc25a12_guide 7:ACTCGCAGTCCCAGTTAAAA	IDT DNA	custom oligo
Recombinant DNA		
pLKO.1:TRCN0000069911 mouse shRNA targetting AGC1 (KD1)	Sigma-Aldrich	Clone ID: NM_172436.2-691s1c1
pLKO.1:TRCN0000069908 mouse shRNA targetting AGC1 (KD2)	Sigma-Aldrich	Clone ID: NM_172436.2-1241s1c1
pLKO.1:TRCN0000069912 mouse shRNA targetting AGC1 (KD3)	Sigma-Aldrich	Clone ID: NM_172436.2-460s1c1
pLKO.1:TRCN0000044591 human shRNA targetting AGC1 (KDa)	Sigma-Aldrich	Clone ID: NM_003705.2-132s1c1
pLKO.1:TRCN0000310089 human shRNA targetting AGC1 (KDb)	Sigma-Aldrich	Clone ID: NM_003705.3-212s21c1
pLKO.1-puro Non-Target shRNA Control	Sigma-Aldrich	Cat #: SHC016V
pLentiCRISPRv2 (lentiviral Cas9 expressing vector)	Laboratory of Dr. Feng Zhang	Addgene Cat #52961
pcDNA4 HisMaxC-mouseAGC1	subcloned into pcDNA4 HisMaxC	N/A
PMXS-SLC1A3	Laboratory of Dr. Kivanc Birsoy	Addgene Cat #72873
Software and Algorithms		
GraphPad Prism 7 for Graphs and statistics	GraphPad Software	https://www.graphpad.com/
Amdis GCMS Data Analysis Software	NIST	N/A
xCalibur Software for LCSM Analysis	Thermo Fisher Scientific	N/A
MATLAB	MathWorks	https://www.mathworks.com/
FlowJo v10 for Flow Cytometry Data Analysis	FlowJo, LLC	https://www.flowjo.com/
Corel Draw x7 for Figure Preparation	Corel Corporation	https://www.coreldraw.com/
Other		
DMEM, High Glucose, Pyruvate	GIBCO	Cat #: 11995065
DMEM W/L-Glutamine and 4.5g/L Glucose; w/ot Sodium Pyruvate	Corning	Cat #: MT10017CV
DMEM, High Glucose, No Glutamine	GIBCO	Cat #: 11960044
DMEM, No Glucose, No Glutamine No Sodium Pyruvate	Corning	Cat #: 17-207-CV
Hank's Balanced Salt Solution	Sigma	Cat #: H8264
Phosphate Buffered Saline (Calcium/Magnesium free)	GIBCO	Ref # 10010-015 500mL

CONTACT FOR REAGENT AND RESOURCE SHARING

Further information and requests for resources and reagents should be directed to the Lead Contact, Juliane G. Bogner-Strauss (juliane.bogner-strauss@tugraz.at).

EXPERIMENTAL MODEL AND SUBJECT DETAILS

Cell Lines

All cells were sub-cultured in Dulbecco's Modified Eagle's Medium (DMEM, (25mM Glucose, 4mM Glutamine, 1mM Sodium Pyruvate) (GIBCO) supplemented with 10% fetal bovine serum and 50units/mL Penicilin/Streptomycin and incubated at 37°C with 5% CO2. All cells utilized tested negative for Mycoplasma. The AL1376 cell line was derived from the KrasG12D; p53fl/fl; Pdx-cre mouse model as described previously (Mayers et al., 2014).

Animals

The study was approved by the institutional ethics committee and experiments were performed according to the guidelines of the Austrian Federal Ministry of Science and Research. Experiment licenses were granted under BMWF-66.007/0026-WF/V/3b/2015 and BMWF-66.007/0008-WF/V/3b/2016. Mouse experiments with CB-839 were approved by the MIT Committee on Animal Care (IACUC). 500,000 LLC1 or 100,000 AL1376 cells were injected into flanks of 7-8 weeks old female C57BL/6 mice (Janvier and Jackson Laboratories). Tumor sizes were measured using calipers throughout the study and estimated volumes were calculated by using the formula V = (π/6)*(length*width^2) (Gui et al., 2016). For CB-839 treatment studies, tumors were grown for 12 or 17 days followed by administration of 200mg/kg CB-839 or vehicle twice daily as previously described (Gross et al., 2014). Tumors were harvested 4 hours after the final drug dose and metabolites were quantified using LCMS.

METHOD DETAILS

Stable-knockdown of AGC1

Stable knock-down of AGC1 protein in cells was achieved by using 5 independent mouse *Slc25a12* mRNA targeting, 2 independent human *SLC25A12* mRNA targeting and 2 mammalian non-targeting lentiviral shRNA particles purchased from Sigma. For the transduction, 5 000 to 10 000 cells/well were seeded into 6-well plates. The following day, fresh media containing virus was added with 8μg/mL Polybrene to each well. One well was incubated without lentivirus for selection control. After 3-4 days, cells were moved to T25 flasks; and selection was performed using varying concentrations of puromycin (ranging from 1μg/mL to 4μg/mL) for 5-7 days until no viable cells remained in selection control.

Proliferation/Survival Rates

25,000 cells/well (long term proliferation/survival experiments) or 100,000-200,000 cells/well (short term starvation, CB-839 treatment) were seeded into 6-well plates. After adhering overnight, initial cell number was determined from reference wells following trypsinization. Then the experimental wells were washed with PBS at least twice or once (only for LLC1 cells) and media conditions were applied. Due to low-adherent nature of LLC1 cells, both PBS and fresh media was applied very carefully. Final cell numbers were counted 2 or 3 days for C2C12 and LLC1 cells and 4 or 7 days AL1376, A549, H1299, PANC1, CAPAN2, HeLa cells after the treatment for proliferation experiments. Minimum 3mL media was used per well, 4 or 5mL media was used for incubations longer than 3 days. Proliferation/survival rate was calculated by the following formula

$$\text{Proliferation/Survival Rate} = \text{Log2}(\text{Final cell count}/\text{Initial cell count})/\text{Day}$$

Cell Viability Assays

500 cells (for proliferation assays) or 2,000 cells (for survival assays) were seeded into 96-well plates and allowed to adhere overnight. Media conditions (100μL/well) were applied as indicated. After media change, 40μL (for survival) or 100μL (for proliferation) Cell Titer Glo (Promega) reagent was added into reference wells to get initial values for each replicate. Manufacturer's recommendations were followed to determine luminescence signals: plates were mixed for 2-3 min, incubated at room temperature for 10 min and signals were measured using a luminometer (Oreon II Microplate Reader Luminometer (Berthold)). The same protocol was used for final day measurements. For survival studies, the final measurement was obtained after two or three days. For growth assays, media was refreshed every second day and final measurements were made at day four or five and growth rate calculated by the following formula:

$$\text{Proliferation/Survival Rate} = \text{Log2}(\text{Final measurement}/\text{Initial measurement})/\text{Day}$$

Determining Annexin V/Propidium Iodide staining using flow cytometry

150,000-200,000 cells were seeded into 6-well plates using full DMEM media. The next day, cells were washed and pyruvate-free DMEM with 4mM or 0.1mM glutamine was added. 24hours later cells were collected via trypsinization and stained with Annexin V and propidium iodide using Thermo Fisher Dead Cell Apoptosis Kit with Annexin V Alexa Fluor 488 & Propidium Iodide (PI) (V13241) to determine dead and apoptotic cells following manufacturer's instructions. Specifically, maximum 1 million/mL cells were diluted with annexin binding buffer after several washing steps and 5μL Alexa Fluor 488-Annexin PI and 1μL 100μg/mL PI solutions were added onto 100μL cell suspensions and incubated at room temperature for 15minutes. After the incubation period, 400μL of Aannexin-binding buffer was mixed gently with the cell suspension and immediately after fluorescence emmisons were measured in FITC (Annexin V) and Texas Red (PI) channels using a flow cytometer (BD, FACS Diva). The percentages of cells positive for either of these dyes were determined and analyzed using FlowJo software.

Transient overexpression of mouse and human AGC1

In order to investigate the effects of transient overexpression of murine AGC1 on proliferation, wild-type C2C12 cells, 0,5x10^5 cells were seeded into 1,5mL fresh media containing 6-well plates together with 1:1 mixture of 0.35μg pcDNA HisMax C vectors with or without AGC1 and 2μL Metafectane Pro (Biontex) -each diluted in 100μL serum free DMEM-. Media was refreshed after 24 hours and cells were counted 60-64 hours after transfection. The proliferation rate was calculated as described above.

To rescue AGC1-KD cells by expressing human AGC1, 70% confluent C2C12 cells were sub-cultured from T-75 flasks into 6-well plates while transfecting pHLCX-flag vectors with or without human AGC1 (hAGC1). 12hours later, 2,000 cells were seeded into 96-well plates for a cell viability assay. Media conditions were applied 8-12 hours later and final measurements were obtained 48hours after the reference measurements, as described above.

CRISPR/Cas9-mediated knock-out of AGC1

7 different guide pairs targeting mouse AGC1 (sgAGC1) were cloned individually into the lentiCRISPRv2 vector (Sanjana et al., 2014; Shalem et al., 2014) that includes a Cas9-expressing cassette. Lentivirus was produced using these vectors, as well as from an empty vector using HEK293T cells as described previously (Sanjana et al., 2014; Shalem et al., 2014). In order to avoid single-cell cloning artifacts, we pooled the vectors containing different sgAGC1 and following lentiviral transduction, C2C12 cells were selected in the presence of 2mM pyruvate and 10mM aspartate.

siRNA-mediated knock-down of Got1/2

Universal Negative Control(SIC001) or MISSION esiRNA targeting mouse Got1 (EMU029631) or mouse Got2 (EMU094111) from Sigma-Aldrich were delivered to C2C12 cells using X-tremeGENE siRNA Transfection Reagent (Roche, 04476093001) following the manufacturer's instructions. Specifically, we gently mixed 100pmol control siRNA or combination of Got1/Got2 esiRNA (50pmol each) with 200μL transfection reagent and applied them onto C2C12 cells that were previously grown to 50%–60% confluency in 6-well plates. 8 hours later, cells were split into new 6-well plates as described for proliferation assays and media conditions were applied 2-hours after all cell plating.

NAD+/NADH Measurements

NAD+/NADH ratio measurement method was adopted from Sullivan et al. (2015). 25,000 cells per well were seeded into 6-well plates using pyruvate-free DMEM, extracted in 120μL 1:1 0.2N NaOH:PBS solution after 24hours and frozen at −80°C immediately. For NADH measurement, 20μL lysate was incubated at 75°C for 30 min, during which oxidized NAD is degraded. For NAD+, 20μL lysate was diluted 1:1 with lysis buffer and 20μL 0.4N HCl was added. Later, NAD+ samples were incubated at 60°C for 15min to selectively degrade the reduced form of NAD. After individual incubations, samples were cooled down to room temperature for 8 min and the degradation reactions were stopped by 20μL 0.25mM Tris in 0.2N HCl (NADH) and 0.5mM Tris base (NAD+). Manufacturer's instruction were followed after sample preparation using the NAD/NADH Glo Assay (Promega).

Mitochondrial Oxygen Consumption

C2C12 cells were seeded in XF96 polystyrene cell culture microplates (Seahorse Bioscience) at a density of 25.000 cells per well. 24 h after plating, cells were washed and preincubated for 30 min in serum-free XF assay medium supplemented with D-glucose (25 mM), sodium pyruvate (1 mM) and glutamine (2 mM) at 37°C in a non-CO2 environment. Oxygen consumption rate (OCR) was subsequently measured every 7 min using an XF96 extracellular flux analyzer (Seahorse Bioscience). 2.5 μM antimycin A was used to stop mitochondrial respiration (= non-mitochondrial respiration). Basal mitochondrial oxygen consumption rate (OCR) was calculated by subtracting average of 3 subsequent non-mitochondrial OCRs from average of three basal OCRs (prior to antimycin treatment) and normalized to individual protein amount (pmol O2/(min x protein per well)).

For CB-839 treatment, 60,000 C2C12 cells were seeded in XF24-well plates and allowed to adhere overnight. The next day, wells were washed twice with PBS and serum-free, pyruvate-free DMEM, in the presence or absence of 1μM CB-839 (or 0.01% DMSO). 6 hours after treatment, OCRs were measured as described above and subsequently normalized to cell counts and OCRs of individual genotype (control versus AGC1-KD) in DMSO treated conditions.

Isotope Tracing and GCMS Analysis

For metabolic tracing studies 150,000-200,000 cells/well were seeded in 6-well plates overnight. Cells were washed three times and 5mM [U-^{13}C]glucose or 4mM [U-^{13}C]glutamine (Cambridge Isotopes Laboratories) containing DMEM (10% dialysed serum, no pyruvate) was applied. After 24h of culture, metabolites were extracted from cells or media (10μL) in 80% methanol in water containing 1μg/sample norvaline and dried under nitrogen gas. Polar metabolites were derivatized and measured as described previously (Lewis et al., 2014). Relative metabolite abundances were calculated by integrating ion peak area and normalized to norvaline and later to the cell numbers from identical plates. Mass isotopomer distributions of each ion peak were determined after natural abundance corrections adapted from Fernandez et al. (1996).

Metabolic profiling using LCMS

For cells: 200,000 (in 6-well plate, for TCA intermediates and amino acids) (Corning) C2C12 cells were starved for glutamine in the absence or presence of 5mM Aspartate for 24hours. Samples were prepared the same way as described in the above GCMS section. For tumors: each tumor was snap-frozen in liquid nitrogen immediately after harvesting and stored at −80°C. 6 tumors per group were selected randomly and ~10-20mg from each tumor was sampled and extracted in 80% methanol following the abovementioned procedure. Metabolites were quantified as detailed previously (Sullivan et al., 2015; Davidson et al., 2016). Briefly, dried polar samples were resuspended in 50 μL water and 2 μL were injected into a ZIC-pHILIC 150 × 2.1 mm (5 μm particle size) column (EMD Millipore). Analysis was conducted on a QExactive benchtop orbitrap mass spectrometer equipped with an Ion Max source and a

HESI II probe, which was coupled to a Dionex UltiMate 3000 UPLC system (Thermo Fisher Scientific, San Jose, CA). External mass calibration was performed using the standard calibration mixture every 7 days. Chromatographic separation was achieved using the following conditions: Buffer A was 20 mM ammonium carbonate, 0.1% ammonium hydroxide; buffer B was acetonitrile. The column oven and autosampler tray were held at 25°C and 4°C, respectively. The chromatographic gradient was run at a flow rate of 0.150 mL/min as follows: 0–20 min.: linear gradient from 80% to 20% B; 20–20.5 min.: linear gradient from 20% to 80% B; 20.5–28 min.: hold at 80% B. The mass spectrometer was operated in full-scan, polarity switching mode with the spray voltage set to 3.0 kV, the heated capillary held at 275°C, and the HESI probe held at 350°C. The sheath gas flow was set to 40 units, the auxiliary gas flow was set to 15 units, and the sweep gas flow was set to 1 unit. MS data acquisition was performed in a range of 70–1000 m/z, with the resolution set at 70,000, the AGC target at 10e6, and the maximum injection time at 20 msec. Relative quantitation of polar metabolites was performed with XCalibur QuanBrowser 2.2 (Thermo Fisher Scientific) using a 5 ppm mass tolerance and referencing an in-house library of chemical standards.

Metabolite Measurements using NMR

Sub-confluent C2C12 or LLC1 cells were incubated in 15cm dishes with pyruvate-free DMEM containing 5mM [U-^{13}C]glucose or 2mM [U-^{13}C]glutamine (Cambridge Isotopes Laboratories) for 12 hours. Next day, cells were washed twice and lysed in PBS via sonication. For quenching the metabolites; one volume of cell lysate (or media) was mixed with two volumes of cold methanol, incubated at −20°C for at least 1 hour, and centrifuged at 13000 rpm for 30 min to pellet proteins. Supernatants were transferred to fresh vials and dried for 4 hours at room temperature using a speed vac. 500 μL of NMR buffer in D_2O were added to the samples, re-dissolved and transferred to 5 mm NMR tubes. Metabolites were measured as described previously (Prokesch et al., 2017; Radović et al., 2016). Briefly, methanol, sodium phosphate, dibasic (Na_2HPO_4), sodium hydroxide, hydrochloric acid (32% m/v), and sodium azide (NaN_3) were obtained from VWR International (Darmstadt, Germany). 3(trimethylsilyl)propionic acid-2,2,3,3-d4 sodium salt (TSP) was obtained from Alfa Aesar (Karlsruhe, Germany). Deuterium oxide (D_2O) was obtained from Cambridge Isotope laboratories (Tewksbury, MA). Deionized water was purified using an inhouse Milli-Q Advantage Water Purification System from Millipore (Schwalbach, Germany). All chemicals were used with no further purification. The phosphate buffer solution was prepared by dissolving 5.56 g of anhydrous NaH_2PO_4, 0.4 g of TSP, and 0.2 g NaN_3, in 400 mL of deionized water and adjusted to pH 7.4 with 1M NaOH and HCl. Upon addition of deionized water to a final volume of 500 mL the pH was readjusted to pH 7.4 with 1M NaOH and HCl. The buffer was lyophilized and taken up in 500 mL D_2O to obtain NMR buffer in D_2O.

All NMR experiments were performed at 310 K on a Bruker Avance III 500 MHz spectrometer equipped with a TXI probe head. The 1D CPMG (Carr−Purcell−Meiboom−Gill) pulse sequence (cpmgpr1d, 512 scans, 73728 points in F1, 12019.230 Hz spectral width, 1024 transients, recycle delay 4 s), with water suppression using pre-saturation, was used for 1H 1D NMR experiments.

Bruker Topspin version 3.1 was used for NMR data acquisition. The spectra for all samples were automatically processed (exponential line broadening of 0.3 Hz), phased, and referenced to TSP at 0.0 ppm using Bruker Topspin 3.1 software (Bruker GmbH, Rheinstetten, Germany).

The 2D HSQC (heteronuclear single quantum correlation) pulse sequence (hsqcetgpsisp2, 8 scans, 256 points in F1, 2048 points in F2, 12658.228 Hz spectral with in F1, 10026.738 Hz spectral width in F2) was used for 2D ^{1}H-^{13}C experiments. Spectral data were transferred to MestreNova 11.0.2 and processed (exponential line broadening of 0.3 Hz), phased, and referenced to TSP. Integral regions for metabolites of interest corresponding to a certain number of protons and for external standard were defined. Integrals were normalized to the number of protons and concentration was determined using external standard concentration. Concentrations of non-labeled compounds were determined using Chenomx NMR Suite 8.2 using internal standard concentration. For fold changes, the integral ratio of labeled versus unlabelled compounds was calculated for each sample and replicates were averaged.

Immunohistochemistry

For AGC1 immunohistochemistry, Aralar B-2 antibody (Santa Cruz, sc-271056) (diluted 1:50 in Antibody Diluent Solution (Dako, S2022)) was applied on tissue slides that had been previously blocked with 3% H_2O_2 in methanol and incubated at room temperature for 1h. Afterward, slides were covered with Rabbit/Mouse Detection Solution (Dako 5007) for 30min and subsequently stained with AEC Substrate Chromogen (Dako, K3464) and hematoxylin. Sections were imaged using light microscopy (Olympus) at the specified magnifications.

Radioactive CO_2 Release

The day before measurements, 250,000 cells/well were plated into 6-well plates. 1.1μCi [U-^{14}C]-glutamine (ARC 0196) was added into each well and wells were covered with Whatman paper soaked with 5M KOH. After incubating for 1h, wells were treated with 200μL of 2.6N $HClO_4$ for another 2h. Later, papers covering individual wells were cut gently and transferred into vials containing 20mL scintillation cocktail. Following rigorous shaking, radioactive carbon units were measured.

Extracellular Flux Analysis

150,000-200,000 cells were seeded into 6-well plates and let adhere overnight. After 2 washes, media conditions were applied (2ml/well) and cell counts were obtained from reference wells. 48 hours later, media samples were collected, centrifuged at top speed and stored at −80°C and final cell count were obtained from respective wells. Glucose, glutamine, lactate and glutamate concentrations were quantified using Metabolic Flux Analyzer (YSI 2900, YSI Life Sciences) in 96-well format.

Western blot analysis

Cells were harvested by scraping with SDS-lysis buffer (50 mM Tris-HCl, pH 6.8, 10% glycerol, 2.5% SDS, cOmplete protease inhibitor cocktail) and samples were digested by benzonase (Merck Millipore). Protein concentrations were determined with the Pierce BCA Protein Assay Kit (Thermo Fisher Scientific). 15-50 μg of protein lysate were loaded into a 10% or 4%–12% BisTris gel (NuPAGE, Invitrogen, Thermo Fisher Scientific), and gels were blotted to nitrocellulose membranes. Membranes were first blocked with 5%BSA in Tris-Buffered Phospohate Saline (TBST) and then incubated with Aralar B-2 (1:1000) (sc271056, Santa Cruz) and anti β-Actin (1:250000) (A5316, Sigma-Aldrich) antibodies (prepared in the same blocking solution) overnight at 4°C. Later, the primary antibodies were conjugated with horseradish peroxidase using secondary antibody (anti-mouse 1:5000) (Dako Österreich GmbH). SuperSignal West Pico Chemiluminescent Substrate (Thermo Fisher Scientific, Waltham, MA, US) was used for detection.

Quantitative Real-Time PCR

PeqGOLD Total RNA Isolation Kit was used to extract RNA from cells (Peqlab). cDNA was synthesized using High Capacity cDNA Reverse Transcription Kit (Applied Biosystems). mRNA expression of individual genes was assessed using SYBR-green based qPCR method (Platinum SYBR Green qPCR SuperMix-UDG with ROX, Invitrogen) on a StepOne Plus Real-Time PCR System (Applied Biosystems) in 96-well format (96x0,2ml Plate, Frosted Subskirted Thin-wall) using 5pmol primer mixture and 5ng cDNA per well. Ct values of every gene first subtracted from the ones of TfIIβ and/or Rplp0 (δCt), then normalized to the mean δCt of control group for every gene (δδCt). Fold changes were calculated using the following formula:

$$\text{Fold change} = 2^{-(\delta\delta Ct)}$$

In experiments without control groups, such as comparing different cell lines, relative δCt values were projected in logarithmic scale, unless indicated otherwise.

Primers were obtained from Primer Bank Database (https://pga.mgh.harvard.edu/primerbank/). Pairs that yield smaller than 200bp amplicons and do not projected to amplify non-spesific regions were selected. Melting curve analysis was performed to verify specificity of the reactions. Primer sequences are available by request.

QUANTIFICATION AND STATISTICAL ANALYSIS

Data are shown as mean ± standard deviation (SD) or mean ± standard error of the mean (SEM). Heat-maps denote medians. Sample size (n) indicates biological replicates within the same experiment. Statistics were calculated using two-tailed paired Student's t test unless indicated otherwise. Non-parametric t test was used when the data within groups are not normally distributed or the sample size is larger than 6, otherwise parametric t test was applied. Significance levels: *$p \leq 0.05$, **$p \leq 0.01$, ***$p \leq 0.001$.

Cell Metabolism, Volume *28*

Supplemental Information

Cytosolic Aspartate Availability Determines Cell Survival When Glutamine Is Limiting

H. Furkan Alkan, Katharina E. Walter, Alba Luengo, Corina T. Madreiter-Sokolowski, Sarah Stryeck, Allison N. Lau, Wael Al-Zoughbi, Caroline A. Lewis, Craig J. Thomas, Gerald Hoefler, Wolfgang F. Graier, Tobias Madl, Matthew G. Vander Heiden, and Juliane G. Bogner-Strauss

Supplementary Information:

Cytosolic aspartate availability determines cell survival when glutamine is limiting

H. Furkan Alkan,[1,2] Katharina E. Walter,[1] Alba Luengo,[2] Corina T. Madreiter-Sokolowski,[3] Sarah Stryeck,[3] Allison N. Lau,[2] Wael Al-Zoughbi,[4] Caroline A. Lewis,[5] Craig J. Thomas,[6,7] Gerald Hoefler,[4,8] Wolfgang F. Graier,[3,8] Tobias Madl,[3,8] Matthew G. Vander Heiden,[2,9,*] and Juliane G. Bogner-Strauss[1,8,10,*]

[1]Institute of Biochemistry, Graz University of Technology, Humboldtstrasse 46/III, 8010 Graz, Austria

[2]The Koch Institute for Integrative Cancer Research and Department of Biology, Massachusetts Institute of Technology, Cambridge, MA 02142, USA

[3]Gottfried Schatz Research Center, Molecular Biology and Biochemistry, Medical University of Graz, Neue Stiftingtalstrasse 6/6, A-8010 Graz, Austria

[4]Diagnostic and Research Institute of Pathology, Medical University of Graz, Neue Stiftingtalstraße 6, A-8010, Graz, Austria

[5]Whitehead Institute for Biomedical Research, 455 Main Street, Cambridge, MA 02142, USA

[6]Division of Preclinical Innovation, National Center for Advancing Translational Sciences, National Institutes of Health, Bethesda, MD, 20892,USA

[7]Lymphoid Malignancies Branch, National Cancer Institute, Bethesda, MD, 20892, USA.

[8]BioTechMed-Graz, Graz, Austria

[9]Dana-Farber Cancer Institute, Boston, MA 02115, USA

[10]Lead Contact

[*]Co-correspondence: juliane.bogner-strauss@tugraz.at, mvh@mit.edu

SUPPLEMENTARY FIGURE LEGENDS

Figure S1 (Related to Figure 1, 2). AGC1 expression supports increased proliferation, NAD+/NADH ratio, and aspartate levels

(A) Schematic showing the canonical Malate-Aspartate Shuttle (MAS).

(B) mRNA expression of MAS components in (left) human cell lines from the Cancer Cell Line Encyclopaedia (CCLE) or (right) in proliferating transformed or non-transformed mouse cell lines determined using qPCR (compared to TfIIb) (n=1).

(C) Proliferation rate of control (NTC) and AGC1 knockdown LLC1 cells (KD1 and KD2). Fold change in viable cell number is presented as percent of non-targeted control (NTC) cells (n=3)

(D) Intracellular NAD+/NADH ratio was determined in pyruvate free DMEM (n=5) for control LLC1 cells (grey) and AGC1-KD1 LLC1 cells (red) described in panel C. Mean ± SEMs are shown.

(E) Pyruvate to lactate ratio was determined for the same cells in panel D grown in pyruvate-free media using GCMS (n=3).

(F) Cellular aspartate and asparagine levels for the same cells in panel D in standard DMEM without pyruvate as measured using GCMS (n=3).

(G) (Top) Proliferation rate of control (C2C12 + Vehicle) and AGC1-overexpressing (C2C12 + mAGC1) C2C12 cells in media without pyruvate. Final cell counts were normalized to initial cell number before transfection (n=3). (Bottom) AGC1 protein expression by Western blot with β-actin expression shown as a loading control.

(H-I) AMP/ATP ratio, NAD+/NADH ratio and Aspartate levels measured in C2C12 cells that (H) transiently overexpressed mouse AGC1 (as in G) or (I) had stable knockdown of AGC1 (n=3).

(J) Aspartate (Asp), asparagine (Asn), alanine (Ala), and glutamate (Glu) levels in C2C12 cells that individually express 2 independent non-targeting shRNA controls (NTC1 and NTC2) or 3 independent shRNAs targeting AGC1 (KD1, KD2 or KD3). n=2 for NTC1, n=1 for all other conditions.

(K) Proliferation/survival rate of control (C2C12 NTC) or AGC1 knockdown cells (C2C12 AGC1-KD1) transfected with empty vector (EV) or with human AGC1 (hAGC1) as indicated. Cells were cultured in vehicle control (DMSO), 1 μM CB-839, or pyruvate-free DMEM media with 0.1mM glutamine (0.1mM Gln) as indicated, and fold change in viable cell number after two days is shown (n=3)

(L) The percent annexin V and/or propidium iodide (PI) positive control (NTC) and AGC1-KD C2C12 and LLC1 cells cultured for 24h in 4mM glutamine or 0.1mM glutamine as indicated was determined by flow cytometry as shown (n=3).

(M) Cleaved caspase 3 protein expression as determined by Western Blot in control (N) or AGC1-knockdown (A) C2C12 and LLC1 cells cultured for 24h in the presence of 4mM glutamine or 0.1mM glutamine without or with 10mM aspartate as indicated is shown. β-actin expression is also shown as a loading control. Data are representative of n=3 experiments.

All panels show mean ± SD unless indicated otherwise. * $p \leq 0.05$, ** $p \leq 0.01$, *** $p \leq 0.001$.

Figure S2 (Related to Figure 3). Glucose and glutamine utilization is minimally affected by AGC1 loss

(A) Relative labeled(^{13}C)/unlabeled(^{12}C) aspartate (Asp) ratio of control (NTC) or AGC1-knockdown (AGC1-KD) C2C12 or LLC1 cells cultured in media with 5mM [U^{13}C]glucose (Glc) or 2mM [U^{13}C]glutamine (Gln) for 12 hours as determined by NMR spectroscopy (n=5).

(B) Labeled (^{13}C) glucose (Glc) uptake and lactate (Lac) release by control (NTC) or AGC1-knockdown (AGC1-KD) C2C12 or LLC1 cells after culture for 12 hours in media with 5mM [U^{13}C]glucose as determined by NMR spectroscopy (n=5).

(C) Labeled (^{13}C) glutamine (Gln) uptake and glutamate (Glu) release by control (NTC) or AGC1-knockdown (AGC1-KD) C2C12 or LLC1 cells after culture for 12 hours in media with 2mM [U^{13}C]glutamine as determined by NMR spectroscopy (n=5).

(D) Schematic showing how Erastin inhibits glutamate export.

(E) Proliferation rate of control (NTC) or AGC1-knockdown (KD1) C2C12 cells cultured in 1μM CB-839 and with varying concentrations of Erastin (n=1).

(F-G) Steady state labelling of the indicated metabolites when (F) C2C12 or (G) LLC1 cells without (+) or with (-) AGC1 knockdown are cultured for 24 hours in the presence of [U^{13}C]glutamine or [U^{13}C]glucose as noted (aspartate (Asp), citrate (Cit), glutamate (Glu), alpha-ketoglutarate (a-KG), malate (Mal), and succinate (Suc)) (n=3).

(H, K) Heatmap showing relative total pool sizes of the indicated metabolites when control (NTC) or AGC1-knockdown (KD) (H) C2C12 and (K) LLC1 cells are cultured in full DMEM-Pyr media for 24h. Data were normalized to cell number and the median relative change compared to NTC are shown (n=3).

(I, L) Heatmap showing relative levels of the indicated metabolite that increase in media after control (NTC) or AGC1-knockdown (I) C2C12 and (L) LLC1 cells are cultured in full DMEM-Pyr for 24 hours. Data normalized to cell number; median relative changes compared to NTC are shown (n=3).

(J, M) Heatmap showing relative levels of the indicated metabolites that decreased in media when control (NTC) or AGC1-knockdown (J) C2C12 and (M) LLC1 cells are cultured in full DMEM-Pyr for 24 hours. Data normalized to cell number; median relative changes compared to NTC are shown (n=3).

All panels show mean ± SEM unless indicated otherwise.

Figure S3 (Related to Figure 4). Cytosolic aspartate delivery improves proliferation/survival when glutamine is limiting

(A) Survival/proliferation rate of control (NTC) and AGC1-knockdown (AGC1-KD) C2C12 cells cultured in pyruvate-free DMEM containing 0.1mM glutamine in the presence and absence of 5mM aspartate as indicated (n=3) mean ± SEM.

(B) Survival/proliferation rate of control (NTC) and ACG1-KD C2C12 cells expressing the plasma membrane aspartate transporter SLC1A3 cultured in pyruvate-free DMEM containing 0.1mM glutamine in the presence and absence of 0.15mM aspartate as indicated (n=3).

(C) (Left) AGC1 protein expression as determined by Western blot (with Vinculin expression as a loading control). (Center) survival/proliferation rate of control (EV, black bars) and CRISPR/Cas9-mediated AGC1 deleted (AGC1 KO, pink bars) C2C12 cells cultured in 4mM glutamine (Gln) with or without 1μM CB-839, or 0.1mM glutamine, with or without 20mM aspartate (Asp) as indicated. (Right) GCMS-measured aspartate levels and pyruvate/lactate (Pyr/Lac) ratio of control (EV) and CRISPR/Cas9-mediated AGC1 deleted C2C12 cells as indicated (n=3).

(D) Schematic showing of the compartment-specific impact of CB-839 on cytosolic or mitochondrial glutamate production and the TCA cycle.

(E) Survival/proliferation rate of control (NTC) and AGC1-KD C2C12 cells cultured in pyruvate-free DMEM containing 4mM or 0.1mM glutamine (Gln) in the presence or absence of 2.5mM sodium pyruvate (Pyr), 5mM aspartate (Asp), 5mM glutamate (Glu), or 2.5mM alanine (Ala) as indicated (n=3).

All panels show mean ± SDs unless indicated otherwise.

Figure S4 (Related to Figure 5). Levels of TCA metabolites and non-essential amino acids in glutamine limiting conditions and following rescue with different substrates

A) GCMS analysis of TCA cycle intermediates and non-essential amino acids (normalized to cell number) from control (N) and AGC1-knockdown (A) C2C12 or LLC1 cells cultured in 4mM glutamine (4mM Q) or 0.1mM glutamine (0.1mM Q) or 4mM glutamine (4mM Q) with 1μM CB-839 for 24h in the presence and absence of 20mM aspartate (Asp), 2mM dimethylaKG (daKG), 2mM dimethlymalate (dMal), or 2mM sodium pyruvate (Pyr) as indicated. Levels shown are relative to control cells cultured in 4mM glutamine (Q) (n=3, means are shown).

B) GCMS analysis of TCA cycle intermediates and non-essential amino acids (normalized to cell number) from control (N) and AGC1-knockdown (A) C2C12 or LLC1 cells cultured with 0.1mM glutamine (0.1mM Q) or with 1μM CB-839 for 24h in the presence and absence of 20mM aspartate (Asp), 2mM dimethylaKG (daKG), 2mM dimethlymalate (dMal), or 2mM sodium pyruvate (Pyr) as indicated. Levels shown are relative to control cells cultured in 0.1mM glutamine or +1μM CB-839 (n=3, means are shown).

C) GCMS analysis of relative aspartate levels (normalized to cell number) from control (NTC) and AGC1-knockdown (AGC1KD1) C2C12 or LLC cells cultured in 4mM glutamine (Q), with 0.1mM glutamine, or with 1μM CB-839 for 24h in the presence and absence of 20mM aspartate (Asp), 2mM dimethylaKG (daKG), or 2mM sodium pyruvate (Pyr) as indicated. (n=3, means are shown).

D) GCMS analysis of relative asparagine levels (normalized to cell number) from control (NTC) and AGC1-knockdown (AGC1KD1) C2C12 or LLC1 cells cultured in 4mM glutamine (Q), with 0.1mM glutamine, or with 1μM CB-839 for 24h in the

presence and absence of 20mM aspartate (Asp), 2mM dimethylaKG (daKG), or 2mM sodium pyruvate (Pyr) as indicated. (n=3, means are shown).

Figure S5 (Related to Figure 6). Cytosolic aspartate is limiting for nucleotide biosynthesis in glutamine-limited conditions

(A) Schematic showing of N-acetlyaspartate synthesis via the enzyme NAT8L.

(B) GCMS analysis of endogenous intracellular N-acetylaspartate (NAA) in control (NTC) and AGC1-knockdown (AGC1KD1) C2C12 and LLC1 cells as indicated. NAA levels in LLC1 cells engineered to express NAT8L to produce NAA is shown as a control. (nd. = not detected) (n=3)

(C) mRNA expressions of genes involved in amino acid metabolism from control (+AGC1) or AGC1-KD (-AGC1) C2C12 or LLC1 cells cultured for 24h in 4mM glutamine (+Gln) or 0.1mM Gln (-Gln) as indicated. Shown is the median fold change in expression of the indicated gene compared to expression in control (NTC) cells cultured in 4mM glutamine (n=3).

(D) Schematic showing how aspartate undergoes transaminations (Got1/2) to support amino acid biosynthesis, provide carbon to the TCA cycle, or oxidize NADH. To produce aspartate, TCA substrates or amino acids also require transamination. Transamination to produce or consume aspartate is inhibited by AOA or by knockdown of aspartate transaminases (siGot1/2).

(E) Proliferation/survival rates of control (NTC) and AGC1-KD C2C12 cells cultured in media with 0.1mM glutamine (Gln) in the presence or absence of 20mM aspartate (Asp), 1mM or 0.1mM of a mixture of non-essential amino acids containing serine, glycine, alanine, aspartate, asparagine, proline, and glutamate (NEAA), 2mM dimethylalpha-ketoglutarate (daKG), with or without 0.3mM AOA as indicated is shown in the left two panels. Shown in the right panel is proliferation/survival rates of

control (NTC) or AGC1-KD C2C12 cells, cultured in 0.1mM glutamine in the presence or absence of 20mM aspartate (Asp), 2mM dimethylalpha-ketoglutarate (daKG), or 2mM sodium pyruvate (Pyr), with or without control siRNA or siRNA targeting Got1 and Got2 (siGot1/2) as indicated. (n=3)

(F) Proliferation/survival rates of control (NTC) and AGC1-KD LLC1 and AL1376 cells cultured in media with 4mM glutamine with the indicated concentration of CB-839 and a 0.1mM mixture of non-essential amino acids, in the presence or absence of 20mM aspartate, 2mM dimethylalpha-ketoglutarate (daKG), 2mM sodium pyruvate with or without 0.3mM AOA (for LLC1 cells) or 1mM AOA (for AL1376 cells) as indicated. (n=3)

(G) Proliferation/survival rate of control (NTC) or ACG1-knockdown (AGC1KD) C2C12 cells cultured in media without (DMSO) or with 1μM CB-839, in the absence or presence of 10mM aspartate (Asp), 10mM asparagine (Asn), or 4mM of both serine and glycine (Ser/Gly) as indicated. (n=5)

(H) (Left) Tracing map showing the relationship between labeled aspartate carbon and the labeling of TCA cycle intermediates. (Right) Relative enrichment of the most abundant TCA intermediate isotopomers that were found to be labeled from [U-^{13}C]aspartate when control (NTC) or AGC1-knockdown (AGC1KD1) C2C12 cells expressing the aspartate/glutamate transporter SLC1A3 were cultured in media containing [U-^{13}C]aspartate and 0.1mM glutamine. Data shown for each species were normalized to enrichment of M+4 aspartate (n=3)

(I) (Left) Tracing map showing the relationship between labeled glutamate carbon and the labeling of TCA cycle intermediates. (Right) Relative enrichment of the most abundant TCA intermediate isotopomers that were found to be labeled from [U-^{13}C]glutamate when control (NTC) or AGC1-knockdown (AGC1KD1) C2C12 cells expressing the aspartate/glutamate transporter SLC1A3 were cultured in media containing [U-

^{13}C]glutamate and 0.1mM glutamine. Data shown for each species were normalized to enrichment of M+5 glutamate (n=3)

(J) Schematic showing how Aspartate contributes to both purine and pyrimidine biosynthesis. R5P, ribose-5-phosphate; Asp, asparate; Fum, fumarate; IMP, inosine monophosphate.

(K) Proliferation/survival rates of control (NTC) and AGC1-KD LLC1 and AL1376 cells cultured in 4mM glutamine with 1μM (LLC1) or 5μM (AL1376) CB-839 in the presence and absence of a mixture of nucleotide precursors (200μM hypoxanthine, 200μM adenine, 200μM guanine, 100μM thymine and 400μM uridine) as indicated. (n=3).

All figures denote mean ± SDs unless indicated otherwise.

Figure S6 (Related to Figure 7). AGC1 knockdown reduces LLC1 allograft tumor growth

(A) Tumor volume over time of allografts generated from control (NTC) and two independent AGC1-knockdown (AGC1-KD1 and AGC1-KD2) LLC1 cell lines implanted into the flanks of C56BL/6 mice (n≥7).

(B) Tumor weights of the LLC1 allografts described in A at the experiment endpoint (day17).

(C) Tumor volume over time of allografts generated from control (NTC) and AGC1-knockdown (AGC1KD1) LLC1 cells implanted into the flanks of C56BL/6 mice that are dosed with vehicle or 200mg/kg/twice daily of CB-839 starting on day 0 as indicated (n≥6).

(D) Relative levels of the indicated non-essential amino acids and TCA intermediates (normalized to valine) from the tumors described in C. Data are presented as relative change compared to vehicle treated NTC control (n≥5), medians are shown.

(E) Tumor volume over time of allografts generated from control (NTC) and AGC1-knockdown (AGC1KD1) AL1376 cells implanted into the flanks of C56BL/6 mice that are dosed with vehicle or 200mg/kg/twice daily of CB-839 as indicated (n≥6). Dosing of vehicle or CB-839 was started on day 16 as indicated.

(F) Growth of tumors derived from the AL1376 cells described in E in C56BL/6 mice flanks that are dosed with vehicle or 200mg/kg/twice daily CB-839 as indicated starting on day 0 (n≥6).

All figures denote mean ± SEMs unless indicated otherwise.

Figure S7 (Related to Figure 7). AGC1 is expressed in mouse and human tumors

(A) Representative immunohistochemistry staining for AGC1 in the indicated human cancer tissues.

(B) Representative immunohistochemistry for AGC1 expression in normal and cancerous human pancreas tissue sections (n=5). AGC1 expression is observed in pancreatic islets [above left], and ductal carcinoma [right; above and below] but not in normal duct [below left].

(C) AGC1 expression assessed by Western blot in normal mouse pancreas and lung tissue as well as in $Kras^{G12D}$, $p53^{-/-}$ lung and pancreatic tumors arising in genetically engineered mouse models involving these organs as indicated.

Figure S1, related to Figure 1,2

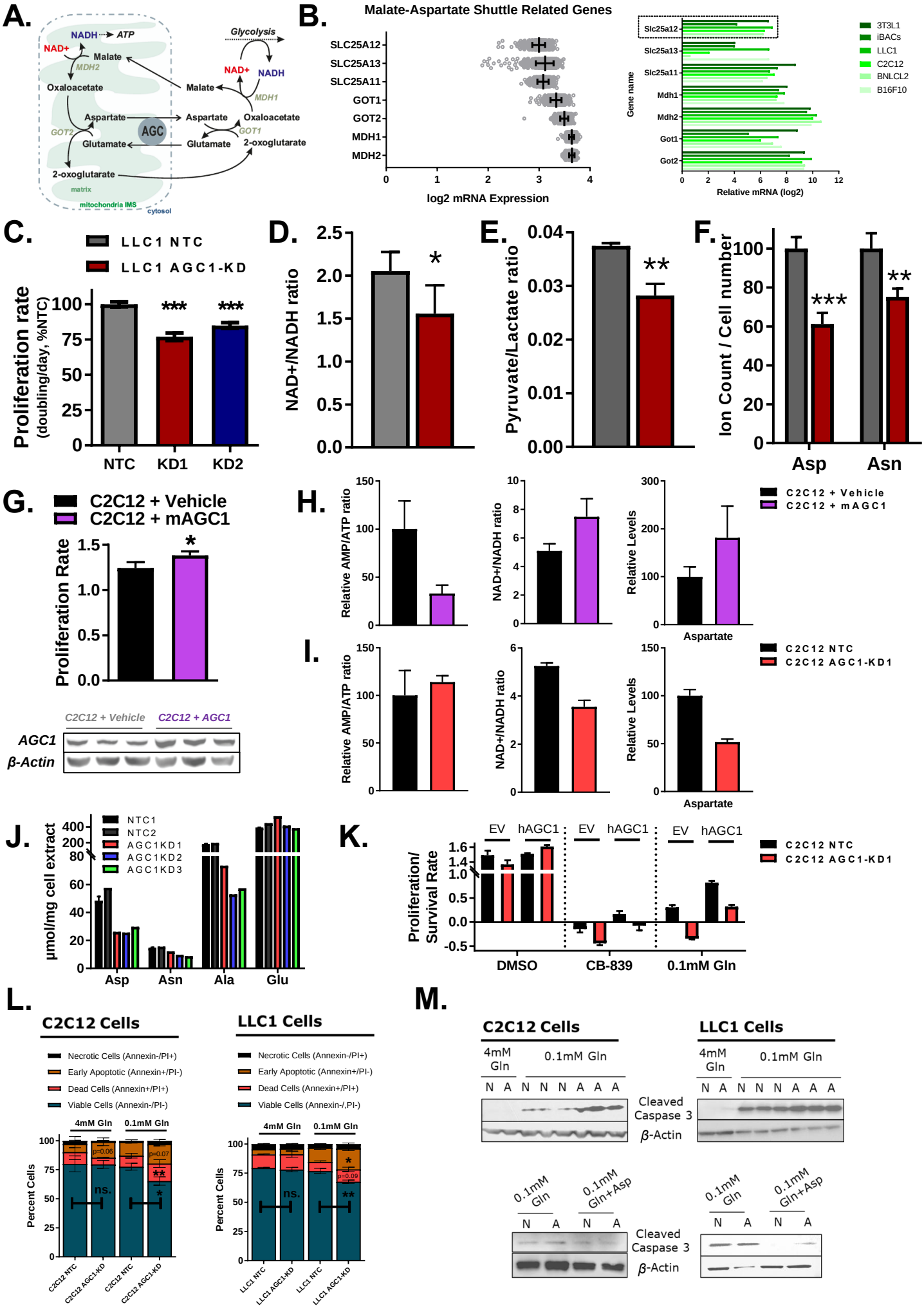

Figure S2, Related to Figure 3

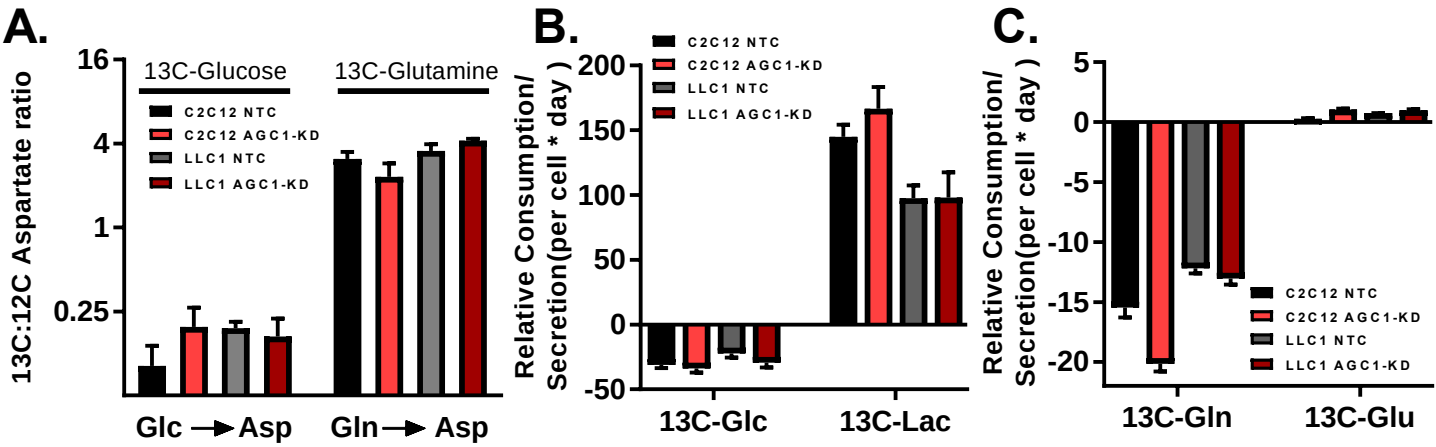

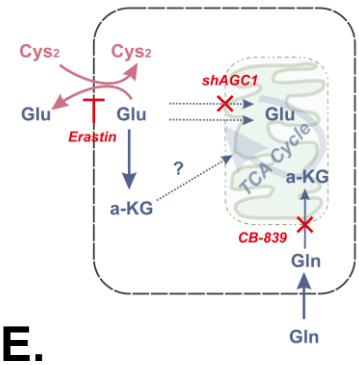

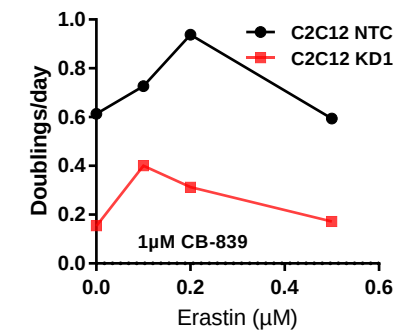

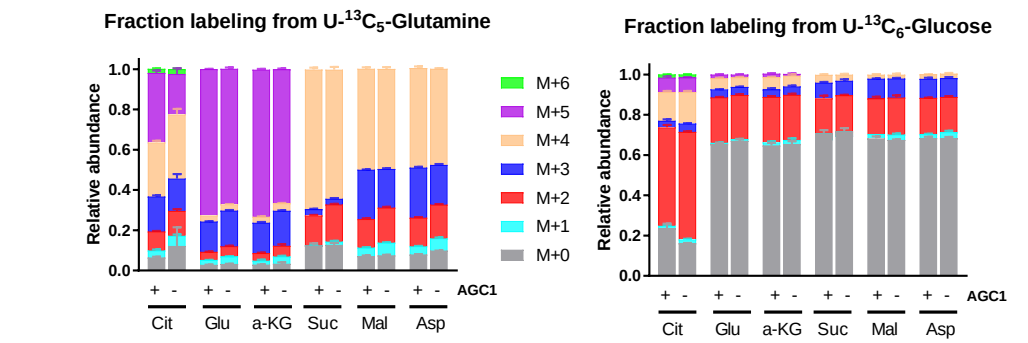

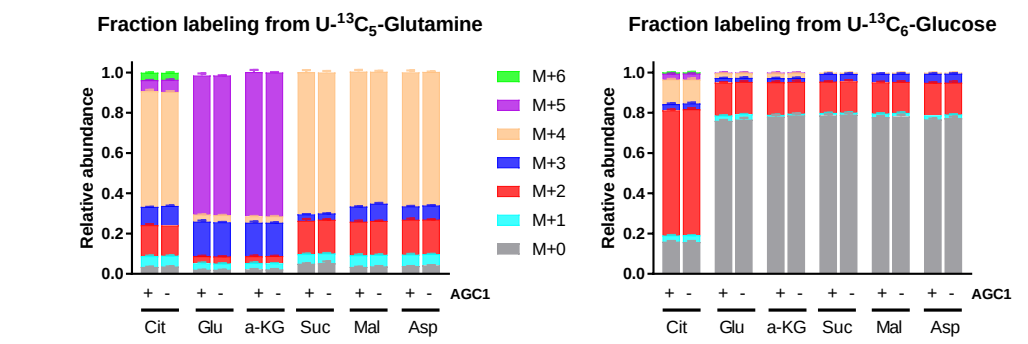

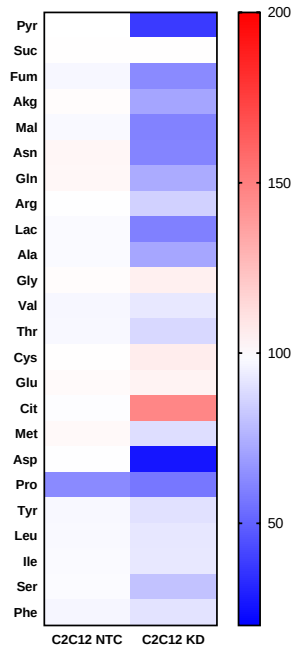

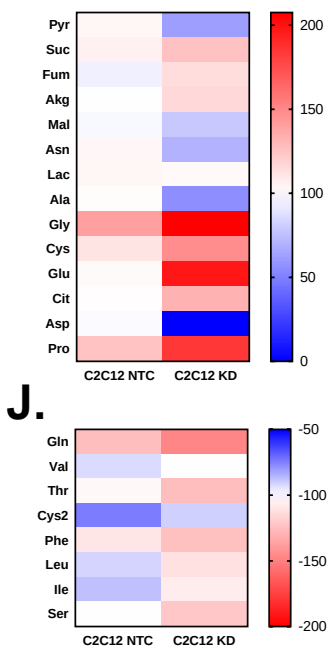

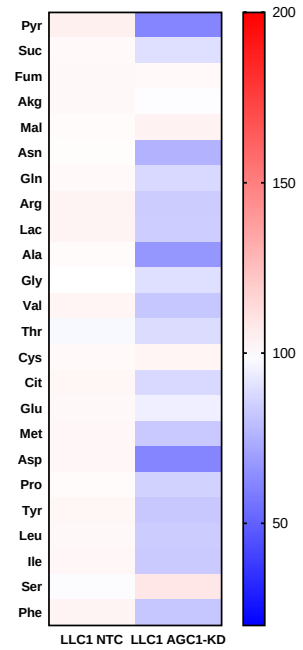

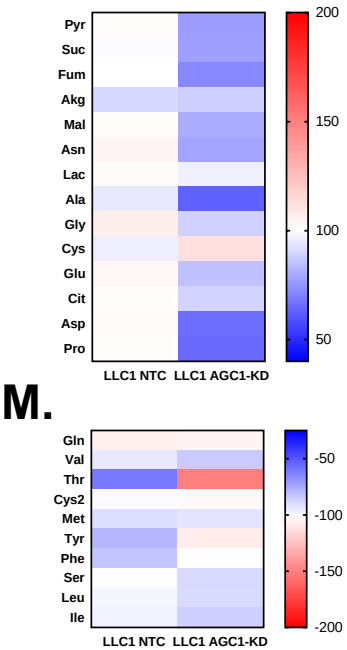

Figure S3, Related to Figure 4

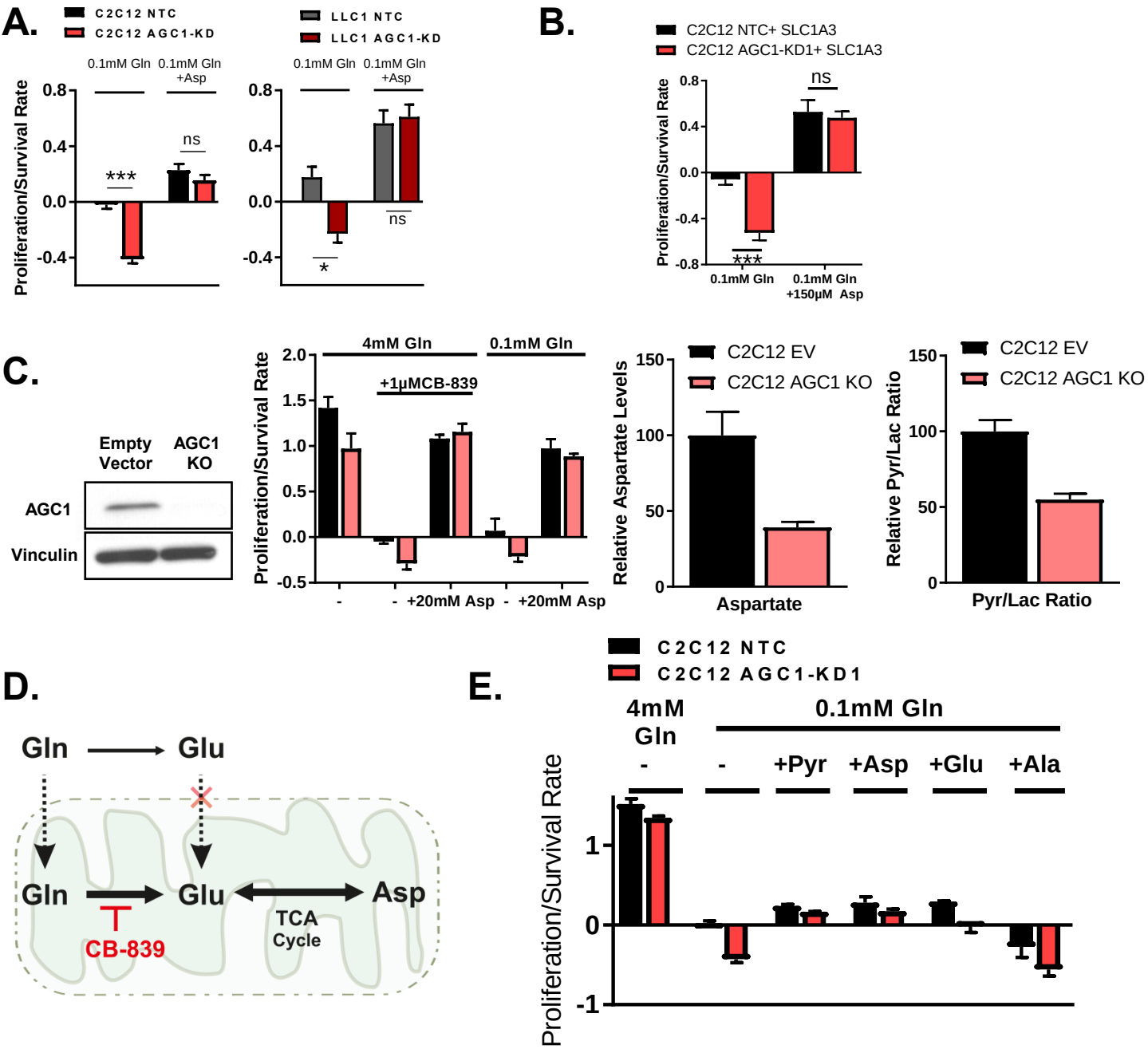

Figure S4, Related to Figure 5

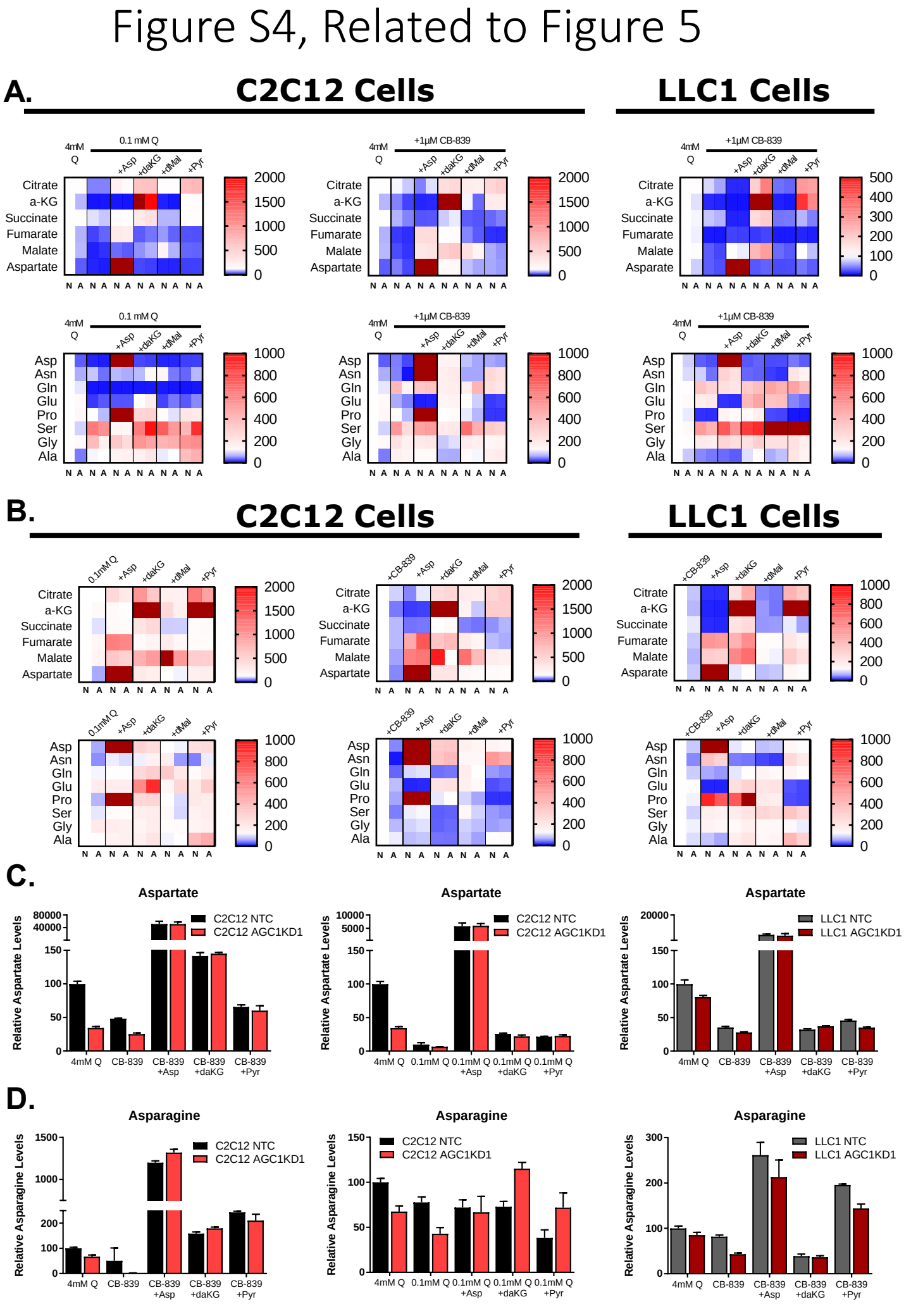

Figure S5, Related to Figure 6

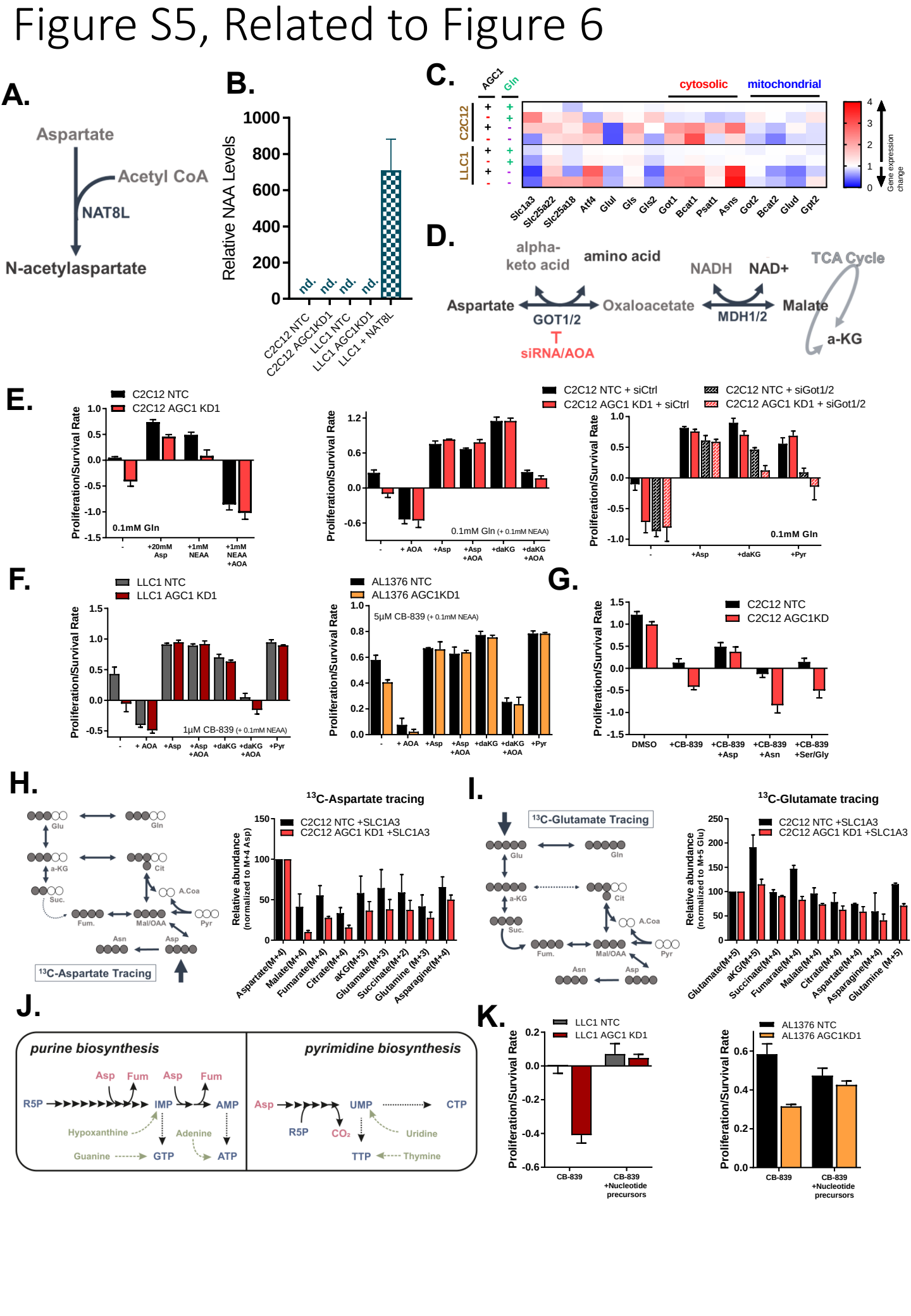

Figure S6, Related to Figure 7

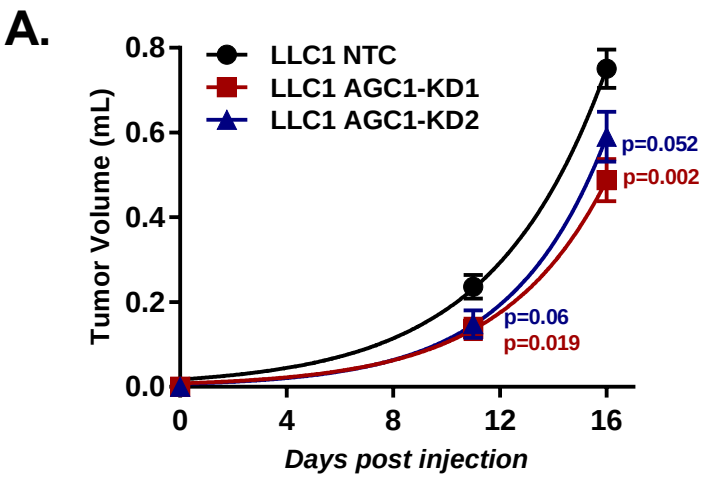

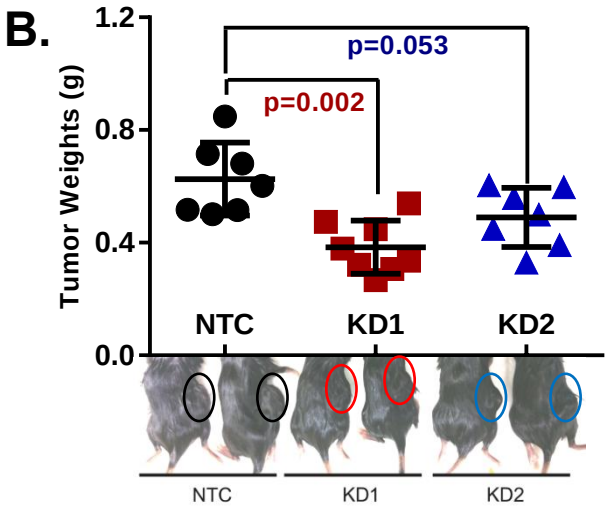

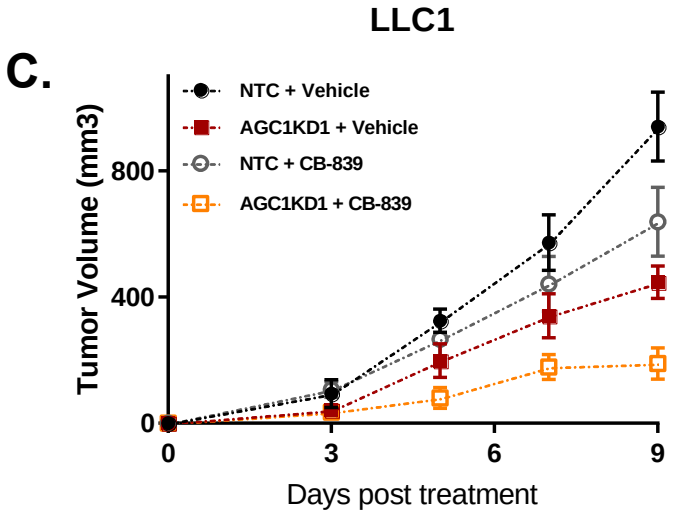

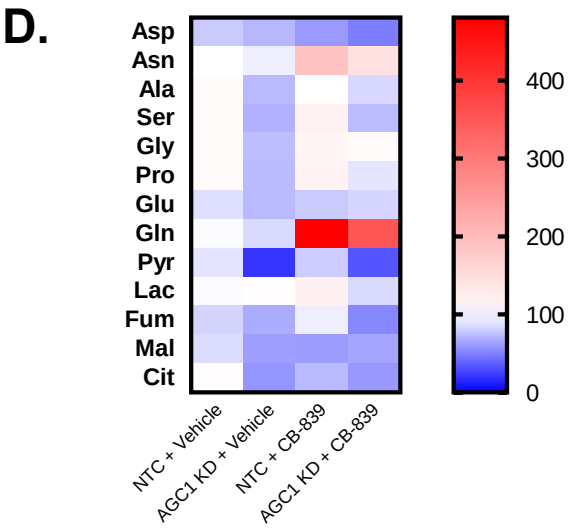

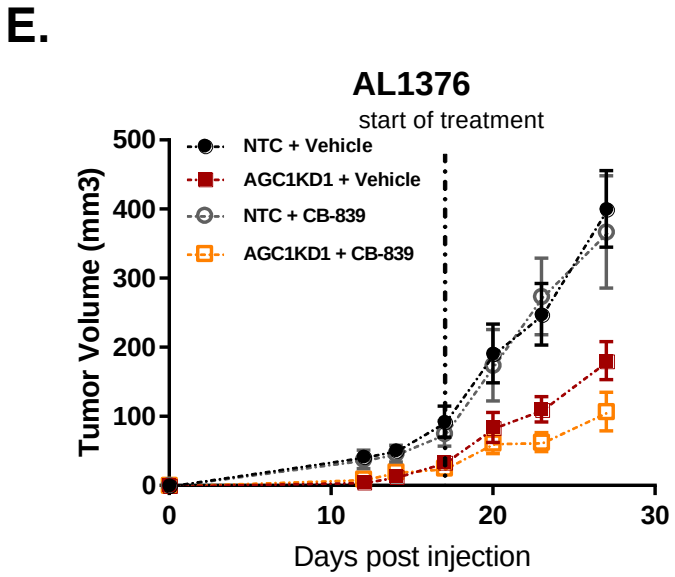

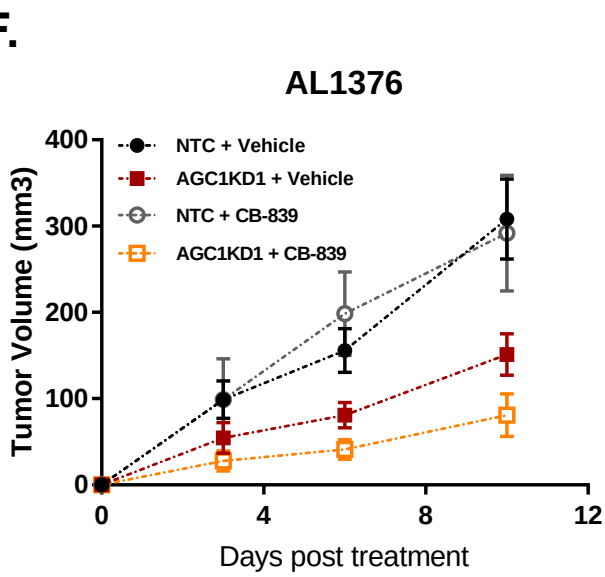

Figure S7, Related to Figure 7